

Wojciech DORNOWSKI, Piotr PERZYNA
Polish Academy of Sciences
Institute of Fundamental Technological Research

LOCALIZATION AND LOCALIZED FRACTURE PHENOMENA IN INELASTIC SOLIDS UNDER CYCLIC DYNAMIC LOADINGS

The main objective of the paper is the investigation of localization and localized fatigue fracture phenomena in thermo-viscoplastic flow processes under cyclic dynamic loadings. Recent experimental observations for cycle fatigue damage mechanics at high temperature and dynamic loadings of metals suggest that the intrinsic microdamage process does very much dependent on the strain rate and the wave shape effects and is mostly developed in the regions where the plastic deformation is localized.

The description of kinematics of finite deformations and the stress tensors is presented. The rates of the deformation tensor and the stress tensor are defined based on the Lie derivative.

A general constitutive model of elasto-viscoplastic damaged polycrystalline solids is developed within the thermodynamic framework of the rate type covariance structure with finite set of the internal state variables. A set of the internal state variables is assumed and interpreted such that the theory developed takes account of the effects as follows: (i) plastic non-normality; (ii) plastic strain induced anisotropy (kinematic hardening); (iii) softening generated by microdamage mechanisms (nucleation, growth and coalescence of microcracks); (iv) thermomechanical coupling (thermal plastic softening and thermal expansion); (v) rate sensitivity; (vi) plastic spin. To describe suitably the time and temperature dependent effects observed experimentally and the accumulation of the plastic deformation and damage during dynamic cyclic loading process the kinetics of microdamage and the kinematic hardening law have been modified. The relaxation time is used as a regularization parameter.

Fracture criterion based on the evolution of microdamage is formulated.

Utilizing the finite difference method for regularized elasto-viscoplastic model, the numerical investigation of the three-dimensional dynamic adiabatic deformation in a particular body under cyclic loading condition is presented. Particular examples have been considered:

(i) Dynamic, adiabatic and isothermal, cyclic loading processes for a thin steel plate with small rectangular hole located in the centre are considered. The accumulation

of damage and equivalent plastic deformation on each considered cycle has been obtained. It has been found that this accumulation distinctly depends on the shape of the assumed loading cycle.

(ii) A dynamic adiabatic cyclic loading process for a thin steel plate with sharp notch is investigated. The propagation of the macroscopic fatigue damage crack within the material of the plate is investigated. It has been found that the length of the macroscopic fatigue damage crack distinctly depends on the wave shape of the assumed loading cycle.

The results obtained are in accord with the experimental observations performed by Sidey and Coffin (1979).

Key words: localization, crack, viscoplasticity, damage, cycle loading

1. INTRODUCTION

The paper aims in the investigations of localization of plastic deformation and localized fracture phenomena in thermo–viscoplastic flow processes under cyclic dynamic loadings.

A number of plasticity models have been recently proposed for cyclic loadings, cf. Auricchio, Taylor and Lubliner (1992), Auricchio and Taylor (1995), Chaboche (1986), Dafalias and Popov (1976), Duszek and Perzyna (1991), Mróz (1967), Ristinmaa (1995), Van der Giessen (1989) and Wang and Ohno (1991). However none of these theories is able to describe properly the mechanism of fatigue damage when time and strain rate effects are important. Such effects have been observed by Sidey and Coffin (1979), cf. chapter 2.

The main objective of the present paper is the development of the thermo–elasto–viscoplasticity theory of damaged polycrystalline solids which takes into account the time and temperature dependent effects observed experimentally and the accumulation of the plastic deformation and damage during dynamic cyclic loading processes. To describe these effects we intend to modify a constitutive model of thermo–elasto–viscoplastic damaged polycrystalline solids developed by Duszek–Perzyna and Perzyna (1994). The main modification concerns the kinetics of microdamage and the kinematic hardening law. Next, we would like to use the developed theory to the investigation of the localization of plastic deformation in complex thermo–elasto–viscoplastic flow processes under cyclic dynamic loadings.

Chapter 3 is devoted to the description of kinematics of finite deformations and the stress tensors. The fundamental measures of total deformation are introduced. The decomposition of the strain tensor into the elastic and viscoplastic part is presented. The rates of the deformation tensor and the stress tensor are defined based on the Lie derivative.

In chapter 4 a general constitutive model of elasto–viscoplastic damaged polycrystalline solids is developed with the thermodynamic framework of the rate

type covariance structure with finite set of the internal state variables. A set of the internal state variables consists of the equivalent plastic deformation, volume fraction porosity and the residual stress (the back stress). The theory developed takes account of the effects as follows: (i) plastic non-normality; (ii) plastic induced anisotropy (kinematic hardening); (iii) plastic spin; (iv) softening generated by microdamage mechanisms; (v) thermomechanical coupling (thermal plastic softening and thermal expansion); (vi) rate sensitivity. The relaxation time is used as a regularization parameter. Fracture criterion based on the evolution of microdamage is formulated.

In chapter 5 the numerical solution of the initial-boundary value problem (evolution problem) is examined. A formulation of an adiabatic inelastic flow process is presented. Basic features of a rate dependent plastic model are discussed. The approximation based on the finite difference method and the discussion of the stability condition are presented. The Lax–Richmyer equivalence theorem is formulated and conditions under which this theorem is valid are discussed.

Chapter 6 is devoted to the numerical investigation of dynamic adiabatic and isothermal, cyclic loading processes for two particular examples.

In chapter 7 the localization of plastic deformation and fatigue damage are investigated.

In chapter 8 the final comments are presented.

2. EXPERIMENTAL AND PHYSICAL MOTIVATIONS

Sidey and Coffin (1979) investigated the mechanisms of fatigue as they bear on fatigue damage at elevated temperature when time and strain rate effects are important. This regime is often referred to as that of time-dependent fatigue.

Test on oxygen-free high conductivity (OFHC) copper at 673 K are examined using unequal strain rates to produce the wave shape. Some typical wave shape are shown in Fig. 1, they include equal–equal, slow–fast and fast–slow. Specimens with a gage length of 12.70 mm and diameter of 6.35 mm were used. Strain-controlled fatigue tests were carried out at 673 K in air with a total strain range of 1.0 percent. In each test the cycle time was kept constant at 600 s but the tensile and compressive strain rates were varied so that a study of wave–shape effects could be made. In the case of the unbalanced loops, the ratio of fast to slow strain rates was fixed at 100 to 1 with the slow strain rate being $1.7 \times 10^{-5} \text{ s}^{-1}$. A strain rate of $3.3 \times 10^{-5} \text{ s}^{-1}$ was used in equal ramp rate tests.

Table 1 shows the number of cycles to failure and the time to failure under the various testing conditions. It can be seen that when the total cycle time is kept constant the number of cycles to failure decreases as the tensile–going strain rate decreases.

Fig. 2 shows the failure crack in the fast–slow test. The crack path is trans-

Table 1. Effect of wave-shape on the number of cycles to failure of OFHC copper at 673 K

Cycle	Slow–Fast	Equal	Fast–Slow
N_f	104	380	1138
$t_f(h)$	17	63	190

granular and has started from the surface. Many transgranular surface cracks had initiated and grown for depths up to 0.5 mm but presumably these had ceased growing when one crack became dominant. No internal intergranular cracks were observed.

In contrast, failure in the slow–fast test was intergranular (Fig. 3). Near the fracture edge, extensive intergranular cracks can be seen which have been opened out by the final failure. Many of these cracks were wedge type, but at higher magnifications linked cavities could be seen. It was noted that cavitation was present throughout the gage length. Thus the failure was typical of that for creep fracture with most of the cracks being orientated at right angles to the applied stress direction. The fracture path in the equal strain rate test was intergranular (Fig. 4). Also internal and short surface intergranular cracks were observed. The surface cracks were about one grain in depth and less numerous than in the slow–fast specimen. There was evidence of cavities either near the fracture or in the bulk of the specimen.

The slow strain rate tension test failed by the propagation of an intergranular crack. Microscopically the specimen was very similar to the equal ramp test with intergranular wedge cracks being situated near the fracture surface and no cracking in the bulk region.

Thus, metallography of the specimen indicated that the decrease in fatigue life was associated with a change in the fracture mode from transgranular to intergranular cracking. Cavity damage occurred only when the tensile–going strain rate was less than the compressive–going strain rate.

Similar results have been obtained for the stainless steel (AISI 304) tested at 923 K in air and vacuum, cf. Sidey and Coffin (1979).

3. KINEMATICS OF FINITE DEFORMATION AND FUNDAMENTAL DEFINITIONS

3.1. Fundamental measures of total deformation

Our notation throughout is as follows: \mathcal{B} and \mathcal{S} are manifolds, points in \mathcal{B} are denoted \mathbf{X} and those in \mathcal{S} by \mathbf{x} . The tangent spaces are written $T_{\mathbf{X}}\mathcal{B}$ and $T_{\mathbf{x}}\mathcal{S}$. Coordinate systems are denoted $\{X^A\}$ and $\{x^a\}$ for \mathcal{B} and \mathcal{S} , respectively, with

corresponding bases \mathbf{E}_A and \mathbf{e}_a and dual bases \mathbf{E}^A and \mathbf{e}^a .

Let us take the Riemannian spaces on manifolds \mathcal{B} and \mathcal{S} , i.e. $\{\mathcal{B}, \mathbf{G}\}$ and $\{\mathcal{S}, \mathbf{g}\}$, the metric tensors \mathbf{G} and \mathbf{g} are defined as follows $\mathbf{G} : T\mathcal{B} \rightarrow T^*\mathcal{B}$ and $\mathbf{g} : T\mathcal{S} \rightarrow T^*\mathcal{S}$, where $T\mathcal{B}$ and $T\mathcal{S}$ denote the tangent bundles of \mathcal{B} and \mathcal{S} , respectively, and $T^*\mathcal{B}$ and $T^*\mathcal{S}$ their dual tangent bundles.

Let the metric tensor G_{AB} be defined by $G_{AB}(\mathbf{X}) = (\mathbf{E}_A, \mathbf{E}_B)_{\mathbf{X}}$, and similarly define g_{ab} by $g_{ab}(\mathbf{x}) = (\mathbf{e}_a, \mathbf{e}_b)_{\mathbf{x}}$, where $(\cdot, \cdot)_{\mathbf{X}}$ and $(\cdot, \cdot)_{\mathbf{x}}$ denote the standard inner products in \mathcal{B} and \mathcal{S} , respectively.

Let

$$\mathbf{x} = \phi(\mathbf{X}, t) \quad (3.1)$$

be regular motion, then $\phi_t : \mathcal{B} \rightarrow \mathcal{S}$ is a C^1 actual configuration (at time t) of \mathcal{B} in \mathcal{S} . The tangent of ϕ is denoted \mathbf{F} and is called the deformation gradient of ϕ ; thus $\mathbf{F} = T\phi$. For $\mathbf{X} \in \mathcal{B}$, we let $\mathbf{F}(\mathbf{X})$ denote the restriction of \mathbf{F} to $T_{\mathbf{X}}\mathcal{B}$.

Thus

$$\mathbf{F}(\mathbf{X}, t) : T_{\mathbf{X}}\mathcal{B} \rightarrow T_{\mathbf{x}=\phi(\mathbf{X}, t)}\mathcal{S} \quad (3.2)$$

is a linear transformation for each $\mathbf{X} \in \mathcal{B}$ and $t \in I \subset \mathbb{R}$. For each $\mathbf{X} \in \mathcal{B}$ there exists an orthogonal transformation $\mathbf{R}(\mathbf{X}) : T_{\mathbf{X}}\mathcal{B} \rightarrow T_{\mathbf{x}}\mathcal{S}$ such that $\mathbf{F} = \mathbf{R} \cdot \mathbf{U} = \mathbf{V} \cdot \mathbf{R}$. Notice that \mathbf{U} and \mathbf{V} operate within each fixed tangent space. We call \mathbf{U} and \mathbf{V} the right and left stretch tensor, respectively. For each $\mathbf{X} \in \mathcal{B}$, $\mathbf{U}(\mathbf{X}) : T_{\mathbf{X}}\mathcal{B} \rightarrow T_{\mathbf{X}}\mathcal{B}$ and for each $\mathbf{x} \in \mathcal{S}$, $\mathbf{V}(\mathbf{x}) : T_{\mathbf{x}}\mathcal{S} \rightarrow T_{\mathbf{x}}\mathcal{S}$.

The material (or Lagrangian) strain tensor $\mathbf{E} : T_{\mathbf{X}}\mathcal{B} \rightarrow T_{\mathbf{X}}\mathcal{B}$ is defined by

$$2\mathbf{E} = \mathbf{C} - \mathbf{I}, \quad (\mathbf{I} \text{ denotes the identity on } T_{\mathbf{X}}\mathcal{B}), \quad (3.3)$$

where

$$\mathbf{C} = \mathbf{F}^T \cdot \mathbf{F} = \mathbf{U}^2 = \mathbf{B}^{-1}. \quad (3.4)$$

The spatial (or Eulerian) strain tensor $\mathbf{e} : T_{\mathbf{x}}\mathcal{S} \rightarrow T_{\mathbf{x}}\mathcal{S}$ is defined by

$$2\mathbf{e} = \mathbf{i} - \mathbf{c}, \quad (\mathbf{i} \text{ denotes the identity on } T_{\mathbf{x}}\mathcal{S}), \quad (3.5)$$

where

$$\mathbf{c} = \mathbf{b}^{-1} \quad \text{and} \quad \mathbf{b} = \mathbf{F} \cdot \mathbf{F}^T = \mathbf{V}^2. \quad (3.6)$$

The various strain tensors can be redefined in terms of pull-back and push-forward operations. For the material strain tensor \mathbf{E} and the spatial strain tensor \mathbf{e} we have

$$\begin{aligned} \mathbf{E}^{\flat} &= \phi^*(\mathbf{e}^{\flat}), & E_{AB}(\mathbf{X}) &= e_{ab}(\mathbf{x})F_A^a(\mathbf{X})F_B^b(\mathbf{X}), \\ \mathbf{e}^{\flat} &= \phi_*(\mathbf{E}^{\flat}), & e_{ab}(\mathbf{x}) &= E_{AB}(\mathbf{X})(\mathbf{F}(\mathbf{X})^{-1})_a^A(\mathbf{F}(\mathbf{X})^{-1})_b^B, \end{aligned} \quad (3.7)$$

where the symbol \flat denotes the index lowering operator.

3.2. Finite elasto–viscoplastic deformation

Motivated by the micromechanics of single crystal plasticity we postulate a local multiplicative decomposition of the form

$$\mathbf{F}(\mathbf{X}, t) = \mathbf{F}^e(\mathbf{X}, t) \cdot \mathbf{F}^p(\mathbf{X}, t), \quad (3.8)$$

where \mathbf{F}^{e-1} is interpreted as the local deformation that releases the stresses from each neighborhood $\mathcal{N}(\mathbf{x}) \subset \phi(\mathcal{B})$ in the current configuration of the body, cf. Fig. 5.

Let us consider a particle X , which at time $t = 0$ occupied the place \mathbf{X} in the reference (material) configuration \mathcal{B} , its current place at time t in the actual (spatial) configuration \mathcal{S} is $\mathbf{x} = \phi(\mathbf{X}, t)$ and its position in the unloaded actual configuration \mathcal{S}' is denoted by \mathbf{y} . Thus we have

$$\mathbf{F}^e : T_{\mathbf{y}}\mathcal{S}' \rightarrow T_{\mathbf{x}}\mathcal{S}, \quad \mathbf{F}^p : T_{\mathbf{X}}\mathcal{B} \rightarrow T_{\mathbf{y}}\mathcal{S}', \quad (3.9)$$

where $T_{\mathbf{y}}\mathcal{S}'$ denotes the tangent space in the unloaded actual configuration \mathcal{S}' . It is noteworthy that \mathbf{F}^e and \mathbf{F}^p defined by (3.9) are linear transformations.

We shall treat the tangent space $T_{\mathbf{y}}\mathcal{S}'$ as an auxiliary tool which helps to define the plastic strain tensors¹.

The plastic strain tensor $\mathbf{E}^p : T_{\mathbf{X}}\mathcal{B} \rightarrow T_{\mathbf{X}}\mathcal{B}$ is defined by

$$\mathbf{E}^p = \frac{1}{2}(\mathbf{C}^p - \mathbf{I}), \quad (3.10)$$

where

$$\mathbf{C}^p = \mathbf{F}^{pT} \cdot \mathbf{F}^p = \mathbf{U}^{p2} = \mathbf{B}^{p-1} \quad \text{and} \quad \mathbf{E}^e \stackrel{\text{def}}{=} \mathbf{E} - \mathbf{E}^p. \quad (3.11)$$

Similarly the elastic strain tensor $\mathbf{e}^e : T_{\mathbf{x}}\mathcal{S} \rightarrow T_{\mathbf{x}}\mathcal{S}$ is defined by

$$\mathbf{e}^e = \frac{1}{2}(\mathbf{i} - \mathbf{c}^e), \quad (3.12)$$

where

$$\mathbf{c}^e = \mathbf{b}^{e-1}, \quad \mathbf{b}^e = \mathbf{F}^e \cdot \mathbf{F}^{eT} = \mathbf{V}^{e2} \quad \text{and} \quad \mathbf{e}^p \stackrel{\text{def}}{=} \mathbf{e} - \mathbf{e}^e. \quad (3.13)$$

It is noteworthy to compare the relation

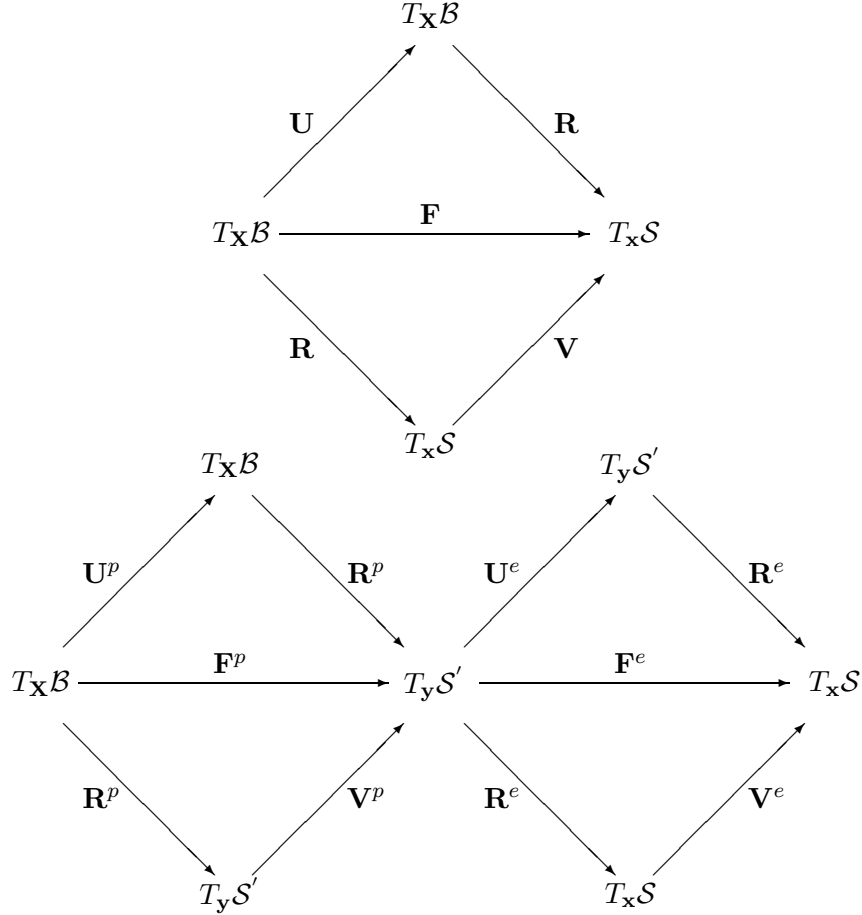
$$\mathbf{F} = \mathbf{R} \cdot \mathbf{U} = \mathbf{V} \cdot \mathbf{R} \quad (3.14)$$

with

$$\mathbf{F} = \mathbf{F}^e \cdot \mathbf{F}^p = \mathbf{R}^e \cdot \mathbf{U}^e \cdot \mathbf{R}^p \cdot \mathbf{U}^p = \mathbf{V}^e \cdot \mathbf{R}^e \cdot \mathbf{V}^p \cdot \mathbf{R}^p. \quad (3.15)$$

The following commutative diagrams summarize the situation.

¹For precise definition of the finite elasto–plastic deformation see Perzyna (1995) and Duszek–Perzyna and Perzyna (1998). Different approach to define the finite elasto–plastic deformation has been presented by Nemat–Nasser (1992).



From the second diagram it is clear that the tangent space $T_y \mathcal{S}'$ is playing an auxiliary role indeed.

The plastic tensors \mathbf{E}^p and \mathbf{e}^p operate within each fixed tangent space; that is $\mathbf{E}^p : T_X \mathcal{B} \rightarrow T_X \mathcal{B}$ and $\mathbf{e}^p : T_x \mathcal{S} \rightarrow T_x \mathcal{S}$.

We can show that the following relations are valid

$$\phi_*(\mathbf{E}^{p^b}) = \mathbf{e}^{p^b}, \quad \phi^*(\mathbf{e}^{e^b}) = \mathbf{E}^{e^b}. \quad (3.16)$$

3.3. Rates of the deformation tensor

Let $\phi(\mathbf{X}, t)$ be a C^2 motion of \mathcal{B} . Then the spatial velocity is $\mathbf{v}_t = \mathbf{V}_t \circ \phi_t^{-1}$, where $\mathbf{V}_t = \frac{\partial \phi}{\partial t}$ is the material velocity, i.e. $\mathbf{v} : \mathcal{S} \times I \rightarrow T\mathcal{S}$, $I \subset \mathbb{R}$.

The collection of maps $\phi_{t,s}$ such that for each s and \mathbf{x} , $t \rightarrow \phi_{t,s}(\mathbf{x})$ is an integral curve of \mathbf{v} , and $\phi_{s,s}(\mathbf{x}) = \mathbf{x}$, is called the flow or evolution operator of \mathbf{v} , i.e.

$$\{\phi_{t,s} \mid \phi_{t,s} = \phi_t \circ \phi_s^{-1} : \phi_s(\mathcal{B}) \rightarrow \phi_t(\mathcal{B})\} \quad (3.17)$$

and

$$\phi_{t,s} \circ \phi_{s,r} = \phi_{t,r}, \quad \phi_{t,t} = \text{identity} \quad (3.18)$$

for all $r, s, t \in I \subset \mathbb{R}$.

If \mathbf{t} is a C^1 (possible time-dependent) tensor field on \mathcal{S} , then the Lie derivative of \mathbf{t} with respect to \mathbf{v} is defined by²

$$\mathbf{L}_{\mathbf{v}}\mathbf{t} = \left(\frac{d}{dt} \phi_{t,s}^* \mathbf{t}_t \right) \Big|_{t=s}. \quad (3.19)$$

If we hold t fixed in \mathbf{t}_t , we obtain the autonomous Lie derivative

$$\mathcal{L}_{\mathbf{v}}\mathbf{t} = \left(\frac{d}{dt} \phi_{t,s}^* \mathbf{t}_s \right) \Big|_{t=s}. \quad (3.20)$$

Thus

$$\mathbf{L}_{\mathbf{v}}\mathbf{t} = \frac{\partial \mathbf{t}}{\partial t} + \mathcal{L}_{\mathbf{v}}\mathbf{t}. \quad (3.21)$$

If $\mathbf{t} \in \mathbf{T}^r_s(\mathcal{S})$ (elements of $\mathbf{T}^r_s(\mathcal{S})$ are called tensors on \mathcal{S} , contravariant of order r and covariant of order s) then $\mathbf{L}_{\mathbf{v}}\mathbf{t} \in \mathbf{T}^r_s(\mathcal{S})$.

The spatial velocity gradient \mathbf{l} is defined by

$$\mathbf{l} = D\mathbf{v} : T_{\mathbf{x}}\mathcal{S} \rightarrow T_{\mathbf{x}}\mathcal{S}, \quad \text{i.e.} \quad l_b^a = v^a \Big|_b = \frac{\partial v^a}{\partial x^b} + \gamma_{bc}^a v^c, \quad (3.22)$$

where γ_{bc}^a denotes the Christoffel symbol for \mathbf{g} .

The spatial velocity gradient \mathbf{l} can be expressed as follows

$$\begin{aligned} \mathbf{l} &= D\mathbf{v} = \dot{\mathbf{F}} \cdot \mathbf{F}^{-1} = \dot{\mathbf{F}}^e \cdot \mathbf{F}^{e-1} + \mathbf{F}^e \cdot (\dot{\mathbf{F}}^p \cdot \mathbf{F}^{p-1}) \cdot \mathbf{F}^{e-1} = \\ &= \mathbf{l}^e + \mathbf{l}^p = \mathbf{d} + \boldsymbol{\omega} = \mathbf{d}^e + \boldsymbol{\omega}^e + \mathbf{d}^p + \boldsymbol{\omega}^p, \end{aligned} \quad (3.23)$$

where \mathbf{d} denotes the spatial rate of deformation tensor and $\boldsymbol{\omega}$ is called the spin.

Let us define the material (or Lagrangian) rate of deformation tensor \mathbf{D} as follows

$$\mathbf{D}(\mathbf{X}, t) = \frac{\partial}{\partial t} \mathbf{E}(\mathbf{X}, t). \quad (3.24)$$

We have very important relation

$$\mathbf{d}^b = \mathbf{L}_{\mathbf{v}}\mathbf{e}^b = \phi_* \frac{\partial}{\partial t} (\phi^* \mathbf{e}^b) = \phi_* \left(\frac{\partial}{\partial t} \mathbf{E}^b \right) = \phi_*(\mathbf{D}^b). \quad (3.25)$$

On the other hand

$$\begin{aligned} \mathbf{d}^b &= \mathbf{L}_{\mathbf{v}}\mathbf{e}^b = \mathbf{L}_{\mathbf{v}} \left[\frac{1}{2} (\mathbf{g} - \mathbf{b}^{-1}) \right]^b = \frac{1}{2} \mathbf{L}_{\mathbf{v}}\mathbf{g} = \\ &= \frac{1}{2} (g_{cb} v^c \Big|_a + g_{ac} v^c \Big|_b) \mathbf{e}^a \otimes \mathbf{e}^b, \end{aligned} \quad (3.26)$$

²The algebraic and dynamic interpretations of the Lie derivative have been presented by Abraham et al. (1988), cf. also Marsden and Hughes (1983).

i.e. the symmetric part of the velocity gradient \mathbf{l} (the symbol \otimes denotes the tensor product).

The components of the spin $\boldsymbol{\omega}$ are given by

$$\omega_{ab} = \frac{1}{2} (g_{ac} v^c|_b - g_{cb} v^c|_a) = \frac{1}{2} \left(\frac{\partial v_a}{\partial x^b} - \frac{\partial v_b}{\partial x^a} \right), \quad (3.27)$$

and

$$\mathbf{d}^{e^b} = \mathbf{L}\mathbf{v}\mathbf{e}^{e^b}, \quad \mathbf{d}^{p^b} = \mathbf{L}\mathbf{v}\mathbf{e}^{p^b}. \quad (3.28)$$

3.4. Rates of the stress tensors

The first Piola–Kirchhoff stress tensor P^{aA} is the two–point tensor obtained by performing a Piola transformation on the second index of the Cauchy stress tensor $\boldsymbol{\sigma}$, i.e.

$$P^{aA} = J(\mathbf{F}^{-1})^A_b \sigma^{ab}, \quad (3.29)$$

where J denotes the Jacobian of the deformation.

The second Piola–Kirchhoff stress tensor \mathbf{S} is defined as follows

$$S^{AB} = (\mathbf{F}^{-1})^A_a P^{aB} = J(\mathbf{F}^{-1})^A_a (\mathbf{F}^{-1})^B_b \sigma^{ab} = (\mathbf{F}^{-1})^A_a (\mathbf{F}^{-1})^B_b \tau^{ab}, \quad (3.30)$$

i.e.

$$\mathbf{S} = \phi^*(\boldsymbol{\tau}), \quad (3.31)$$

where $\boldsymbol{\tau} = J\boldsymbol{\sigma}$ is called the Kirchhoff stress tensor.

The rate of the Kirchhoff stress tensor $\boldsymbol{\tau}$ is given by

$$\mathbf{L}\mathbf{v}\boldsymbol{\tau} = \phi_* \frac{\partial}{\partial t} (\phi^* \boldsymbol{\tau}) = \phi_* \left(\frac{\partial}{\partial t} \mathbf{S} \right) = \mathbf{F} \cdot \left(\frac{\partial}{\partial t} \mathbf{S} \right) \cdot \mathbf{F}^T \circ \phi_t^{-1}. \quad (3.32)$$

Let us define

$$\begin{aligned} \boldsymbol{\tau}_1 &= \tau^{ab} \mathbf{e}_a \otimes \mathbf{e}_b \in \mathbf{T}^2_0(\mathcal{S}), \\ \boldsymbol{\tau}_2 &= \tau_a{}^b \mathbf{e}^a \otimes \mathbf{e}_b \in \mathbf{T}^1_1(\mathcal{S}), \\ \boldsymbol{\tau}_3 &= \tau^a{}_b \mathbf{e}_a \otimes \mathbf{e}^b \in \mathbf{T}^1_1(\mathcal{S}). \end{aligned} \quad (3.33)$$

Then

$$(\mathbf{L}\mathbf{v}\boldsymbol{\tau}_1)^{ab} = \frac{\partial \tau^{ab}}{\partial t} + \frac{\partial \tau^{ab}}{\partial x^c} v^c - \tau^{cb} \frac{\partial v^a}{\partial x^c} - \tau^{ac} \frac{\partial v^b}{\partial x^c}. \quad (3.34)$$

is the rate associated with the name Oldroyd (cf. Oldroyd (1950)). The Zaremba–Jaumann rate (cf. Zaremba (1903a,b) and Jaumann (1911)) is defined as follows

$$\frac{1}{2} \left[(\mathbf{L}\mathbf{v}\boldsymbol{\tau}_3)^a{}_c g^{cb} + g^{ac} (\mathbf{L}\mathbf{v}\boldsymbol{\tau}_2)^c{}_b \right] = \frac{\partial \tau^{ab}}{\partial t} + \frac{\partial \tau^{ab}}{\partial x^c} v^c + \tau^{ad} \omega_d{}^b - \tau^{db} \omega^a{}_d. \quad (3.35)$$

4. CONSTITUTIVE MODELLING FOR DYNAMIC CYCLIC LOADINGS

4.1. Constitutive postulates

Constitutive theory is given most conveniently in the material picture because the domain \mathcal{B} of the functions remains fixed. This helps to develop the identification procedure. However, it can be done spatially as well.

We introduce the four fundamental postulates:

- (i) Existence of the free energy function. It is assumed that the free energy function is given by

$$\psi = \hat{\psi}(\mathbf{e}, \mathbf{F}, \vartheta; \boldsymbol{\mu}), \quad (4.1)$$

where \mathbf{e} denotes the Eulerian strain tensor, \mathbf{F} is deformation gradient, ϑ temperature and $\boldsymbol{\mu}$ denotes a set of the internal state variables.

- (ii) Axiom of objectivity (spatial covariance). The constitutive structure should be invariant with respect to any diffeomorphism $\boldsymbol{\xi} : \mathcal{S} \rightarrow \mathcal{S}$ (Marsden and Hughes, 1983). Assuming that $\boldsymbol{\xi} : \mathcal{S} \rightarrow \mathcal{S}$ is a regular, orientation preserving map transforming \mathbf{x} into \mathbf{x}' and $T\boldsymbol{\xi}$ is an isometry from $T_{\mathbf{x}}\mathcal{S}$, to $T_{\mathbf{x}'}\mathcal{S}$ we obtain the axiom of material frame indifference.

Let us take again $\mathbf{t} \in \mathbf{T}^r_s(\mathcal{S})$ a given time dependent spatial tensor field on \mathcal{S} and let $\boldsymbol{\xi}$ be a diffeomorphism of \mathcal{S} to another manifold $\boldsymbol{\xi}(\phi(\mathcal{B}))$. Any spatial tensor field $\mathbf{t} \in \mathbf{T}^r_s(\mathcal{S})$ is said to transform objectively under superposed diffeomorphism $\boldsymbol{\xi}$ if it transforms according to the rule

$$\mathbf{t}' = \boldsymbol{\xi}_* \mathbf{t}, \quad (4.2)$$

where $\boldsymbol{\xi}_*$ is the push-forward operation.

Let \mathbf{v}' be the velocity field of $\boldsymbol{\xi}_t \circ \phi_t$. Then we have (cf. Marsden and Hughes, 1983)

$$L_{\mathbf{v}'} \mathbf{t}' = \boldsymbol{\xi}_*(L_{\mathbf{v}} \mathbf{t}). \quad (4.3)$$

This means that objective tensors have objective Lie derivatives. It is noteworthy to recall here that rates which are objective with respect to diffeomorphisms are called covariant.

The Oldroyd rate of the Kirchhoff stress tensor (3.34) is objective with respect to diffeomorphisms while the Zaremba–Jaumann rate (3.35) is objective with respect to isometries. The reason of it is caused by the fact that the operations of raising and lowering indices do not commute with Lie differentiation. This corollary has very important consequences for the formulation of the objective constitutive structures.

Before the formulation of the third axiom let us discuss thermodynamic restrictions. Consider balance principles as follows:

1. Conservation of mass. Let assume that $\phi(\mathbf{X}, t)$ is a C^1 regular motion. A mass density function $\rho(\mathbf{x}, t)$ is said to obey conservation of mass if

$$\dot{\rho} + \rho \operatorname{div} \mathbf{v} = 0 \quad \text{or} \quad \rho(\mathbf{x}, t) J(\mathbf{X}, t) = \rho_{Ref}(\mathbf{X}). \quad (4.4)$$

For damaged solid body the mass density $\rho(\mathbf{x}, t)$ is given by

$$\rho = \rho_M(1 - \xi) + \rho_V \xi, \quad (4.5)$$

where ρ_M is the mass density of the matrix material and ρ_V the mass density of voids. Assuming $\rho_V \ll \rho_M$ we have

$$\rho = \rho_M(1 - \xi). \quad (4.6)$$

Thus a function $\rho(\mathbf{x}, t)$ is said to obey conservation of mass if

$$\rho_M(1 - \xi) J(\mathbf{X}, t) = \rho_M^0(\mathbf{X}) (1 - \xi_0) = \rho_{Ref}. \quad (4.7)$$

2. Balance of momentum. Assume that conservation of mass and balance of momentum hold. If there is no external body force field, then

$$\rho \dot{\mathbf{v}} = \operatorname{div} \left(\frac{1}{J} \boldsymbol{\tau} \right). \quad (4.8)$$

3. Balance of moment of momentum. Let conservation of mass and balance of momentum hold. Then balance of moment of momentum holds if and only if $\boldsymbol{\tau}$ is symmetric.
4. Balance of energy. Assume the following balance principle hold: conservation of mass, balance of momentum, balance of moment of momentum and balance of energy. If there is no external heat supply then

$$\rho(\dot{\psi} + \vartheta \dot{\eta} + \eta \dot{\vartheta}) + \operatorname{div} \mathbf{q} = \frac{\rho}{\rho_{Ref}} \boldsymbol{\tau} : \mathbf{d}, \quad (4.9)$$

where η denotes the specific (per unit mass) entropy and \mathbf{q} is the heat vector field.

5. Entropy production inequality. Assume conservation of mass, balance of momentum, moment of momentum, energy and entropy production inequality hold. Then the reduced dissipation inequality is satisfied:

$$\frac{1}{\rho_{Ref}} \boldsymbol{\tau} : \mathbf{d} - (\eta \dot{\vartheta} + \dot{\psi}) - \frac{1}{\rho \vartheta} \mathbf{q} \cdot \operatorname{grad} \vartheta \geq 0. \quad (4.10)$$

- (iii) The axiom of entropy production. For any regular process $\phi_t, \vartheta_t, \boldsymbol{\mu}_t$ of a body \mathcal{B} the constitutive functions are assumed to satisfy the reduced dissipation inequality (4.10). Marsden and Hughes (1983) proved that the reduced dissipation inequality (4.10) is equivalent to the entropy production inequality first introduced by Coleman and Noll (1963) in the form of the Clausius–Duhem inequality. In fact the Clausius–Duhem inequality gives a statement of the second law of thermodynamics within the framework of mechanics of continuous media.
- (iv) The evolution equation for the internal state variable vector $\boldsymbol{\mu}$ is assumed in the form as follows

$$\mathbf{L}_V \boldsymbol{\mu} = \hat{\mathbf{m}}(\mathbf{e}, \mathbf{F}, \vartheta, \boldsymbol{\mu}), \quad (4.11)$$

where the evolution function $\hat{\mathbf{m}}$ has to be determined based on careful physical interpretation of a set of the internal state variables and analysis of available experimental observations.

The determination of the evolution function $\hat{\mathbf{m}}$ (in practice a finite set of the evolution functions) appears to be the main problem of the modern constitutive modelling.

4.2. Fundamental assumptions

The main objective is to develop the rate type constitutive structure for an elastic–viscoplastic material in which the effects of the plastic non–normality, plastic spin, plastic strain induced anisotropy (kinematic hardening), micro–damaged mechanism and thermomechanical coupling are taken into consideration. To do this it is sufficient to assume a finite set of the internal state variables. Let us postulate

$$\boldsymbol{\mu} = (\zeta, \xi, \boldsymbol{\alpha}), \quad (4.12)$$

where ζ denotes the new internal state vector which describes the dissipation effects generated by viscoplastic flow phenomena, ξ is volume fraction porosity and takes account for micro–damaged effects and $\boldsymbol{\alpha}$ denotes the residual stress (the back stress) and aims at the description of the kinematic hardening effects.

Let us introduce the plastic potential function $f = f(\tilde{J}_1, \tilde{J}_2, \vartheta, \boldsymbol{\mu})$, where \tilde{J}_1, \tilde{J}_2 denote the first two invariants of the stress tensor $\tilde{\boldsymbol{\tau}} = \boldsymbol{\tau} - \boldsymbol{\alpha}$.

Let us postulate the evolution equations as follows

$$\mathbf{d}^p = \Lambda \mathbf{P}, \quad \boldsymbol{\omega}^p = \Lambda \boldsymbol{\Omega}, \quad \mathbf{L}_V \zeta = \Lambda \mathbf{Z}, \quad \dot{\xi} = \Xi, \quad \mathbf{L}_V \boldsymbol{\alpha} = \mathbf{A}, \quad (4.13)$$

where for elasto–viscoplastic model of a material we assume (cf. Perzyna (1963, 1966, 1971, 1995))

$$\Lambda = \frac{1}{T_m} \langle \Phi \left(\frac{f}{\kappa} - 1 \right) \rangle, \quad (4.14)$$

T_m denotes the relaxation time for mechanical disturbances, the isotropic work-hardening–softening function κ is

$$\kappa = \hat{\kappa}(\epsilon^p, \vartheta, \xi), \quad \epsilon^p = \int_0^t \left(\frac{2}{3} \mathbf{d}^p : \mathbf{d}^p \right)^{\frac{1}{2}} dt, \quad (4.15)$$

Φ is the empirical overstress function, the bracket $\langle \cdot \rangle$ defines the ramp function,

$$\mathbf{P} = \frac{\partial f}{\partial \boldsymbol{\tau}} \Big|_{\xi=const} \left(\left\| \frac{\partial f}{\partial \boldsymbol{\tau}} \right\| \right)^{-1}, \quad (4.16)$$

$\boldsymbol{\Omega}$, \mathbf{Z} , Ξ and \mathbf{A} denote the evolution functions which have to be determined.

It is noteworthy that the material function \mathbf{Z} is intrinsically determined by the constitutive assumptions postulated. To show this it is sufficient to perform a Legendre transformation as has been presented by Duszek and Perzyna (1991b).

For our practical purposes it is sufficient to assume that the internal state vector $\boldsymbol{\zeta}$ is equal to the equivalent plastic deformation ϵ^p , i.e.

$$\boldsymbol{\mu} = (\epsilon^p, \xi, \boldsymbol{\alpha}). \quad (4.17)$$

Then the material function Z is directly determined from

$$\dot{\epsilon}^p = \Lambda Z = \left(\frac{2}{3} \mathbf{d}^p : \mathbf{d}^p \right)^{\frac{1}{2}} = \sqrt{\frac{2}{3}} \Lambda, \quad (4.18)$$

i.e.

$$Z = \sqrt{\frac{2}{3}}. \quad (4.19)$$

4.3. Constitutive assumption for the plastic spin

The constitutive laws for the plastic spin³ based on the application of the tensor function formulation have been proposed by Mandel (1971, 1973), Kratochvil (1971), Dafalias (1983, 1985, 1987, 1988) and Loret (1983, 1985). Different proposition by using generalized normality condition has been introduced by Halphen (1975), Mandel (1982), Dafalias (1984) and Van der Giessen (1989).

Let us postulate that $\boldsymbol{\Omega}$ has the form (cf. Dafalias, 1983 and Loret, 1983)

$$\boldsymbol{\Omega} = \eta^*(\boldsymbol{\alpha} \cdot \mathbf{P} - \mathbf{P} \cdot \boldsymbol{\alpha}), \quad (4.20)$$

where η^* denotes the scalar valued function of the invariants of the tensors $\boldsymbol{\alpha}$ and \mathbf{P} , and may depend on temperature ϑ and porosity ξ .

³For a thorough discussion of a concept of the plastic spin and its constitutive description in phenomenological theories for macroscopic large plastic deformations please consult the critical review paper by Van der Giessen (1991).

4.4. Intrinsic micro–damage process

An analysis of the experimental observations for cycle fatigue damage mechanisms at high temperature of metals performed by Sidey and Coffin (1979) suggests that the intrinsic micro–damage process does very much depend on the strain rate effects as well as on the wave shape effects, cf. chapter 2.

To take into consideration these observed time dependent effects it is advantageous to use the proposition of the description of the intrinsic micro–damage process presented by Perzyna (1986a,b) and Duszek–Perzyna and Perzyna (1994).

Let us assume that the intrinsic micro–damage process consists of the nucleation and growth mechanism⁴.

Physical considerations (cf. Curran et al. (1987) and Perzyna (1986a)) have shown that the nucleation of microvoids in dynamic loading processes which are characterized by very short time duration is governed by the thermally–activated mechanism. Based on this heuristic suggestion and taking into account the influence of the stress triaxiality on the nucleation mechanism we postulate for rate dependent plastic flow

$$\left(\dot{\xi}\right)_{nucl} = \frac{1}{T_m} h^*(\xi, \vartheta) \left[\exp \frac{m^*(\vartheta) |\tilde{I}_n - \tau_n(\xi, \vartheta, \epsilon^p)|}{k\vartheta} - 1 \right], \quad (4.21)$$

where k denotes the Boltzmann constant, $h^*(\xi, \vartheta)$ represents a void nucleation material function which is introduced to take account of the effect of microvoid interaction effect, $m^*(\vartheta)$ is a temperature dependent coefficient, $\tau_n(\xi, \vartheta, \epsilon^p)$ is the porosity, temperature and equivalent plastic strain dependent threshold stress for microvoid nucleation,

$$\tilde{I}_n = a_1 \tilde{J}_1 + a_2 \sqrt{\tilde{J}_2} + a_3 \left(\tilde{J}_3\right)^{\frac{1}{3}} \quad (4.22)$$

defines the stress intensity invariant for nucleation, a_i ($i = 1, 2, 3$) are the material constants, \tilde{J}_1 denotes the first invariant of the stress tensor $\tilde{\tau} = \tau - \alpha$, \tilde{J}_2 and \tilde{J}_3 are the second and third invariants of the stress deviator $\tilde{\tau}' = (\tau - \alpha)'$.

For the growth mechanism we postulate (cf. Carroll and Holt (1972), Johnson (1981); Perzyna (1986a,b, 1990); Perzyna and Drabik (1989, 2001))

$$\left(\dot{\xi}\right)_{grow} = \frac{1}{T_m} \frac{g^*(\xi, \vartheta)}{\sqrt{\kappa_0}} \left[\tilde{I}_g - \tau_{eq}(\xi, \vartheta, \epsilon^p) \right], \quad (4.23)$$

where $T_m \sqrt{\kappa_0}$ denotes the dynamic viscosity of a material, $g^*(\xi, \vartheta)$ represents a void growth material function and takes account for void interaction, $\tau_{eq}(\xi, \vartheta, \epsilon^p)$

⁴Recent experimental observation results (cf. Shockey et al. (1985)) have shown that coalescence mechanism can be treated as nucleation and growth process on a smaller scale. This conjecture simplifies very much the description of the intrinsic micro–damage process by taking account only of the nucleation and growth mechanisms.

is the porosity, temperature and equivalent plastic strain dependent void growth threshold stress,

$$\tilde{I}_g = b_1 \tilde{J}_1 + b_2 \sqrt{\tilde{J}_2} + b_3 \left(\tilde{J}_3' \right)^{\frac{1}{3}}, \quad (4.24)$$

defines the stress intensity invariant for growth and b_i ($i = 1, 2, 3$) are the material constants.

Finally the evolution equation for the porosity ξ has the form

$$\begin{aligned} \dot{\xi} = & \frac{h^*(\xi, \vartheta)}{T_m} \left[\exp \frac{m^*(\vartheta) |\tilde{I}_n - \tau_n(\xi, \vartheta, \epsilon^p)|}{k\vartheta} - 1 \right] + \\ & + \frac{g^*(\xi, \vartheta)}{T_m \sqrt{\kappa_0}} [\tilde{I}_g - \tau_{eq}(\xi, \vartheta, \epsilon^p)]. \end{aligned} \quad (4.25)$$

This determines the evolution function Ξ .

To have consistent theory of elasto–viscoplasticity we can replace the exponential function in the nucleation term and the linear function in the growth term by the empirical overstress function Φ , then the evolution equation for the porosity ξ takes the form as follows

$$\begin{aligned} \xi^* = & \frac{1}{T_m} h^*(\xi, \vartheta) \langle \Phi \left[\frac{\tilde{I}_n}{\tau_n(\xi, \vartheta, \epsilon^p)} - 1 \right] \rangle + \\ & + \frac{1}{T_m} g^*(\xi, \vartheta) \langle \Phi \left[\frac{\tilde{I}_g}{\tau_{eq}(\xi, \vartheta, \epsilon^p)} - 1 \right] \rangle. \end{aligned} \quad (4.26)$$

4.5. Kinematic hardening

For a constitutive model describing the behaviour of a material under cyclic loading processes the crucial role plays the evolution equation for the back stress α , which is responsible for the description of the induced plastic strain anisotropy effects.

We shall follow some fundamental results obtained by Duszek and Perzyna (1991a) (cf. also Duszek and Perzyna (1988a,b)). Let us postulate

$$L_{\mathbf{v}} \alpha = A(\mathbf{d}^p, \tilde{\tau}, \vartheta, \xi). \quad (4.27)$$

Making use of the tensorial representation of the function A and taking into account that there is no change of α when $\tilde{\tau} = 0$ and $\mathbf{d}^p = 0$ the evolution law (4.27) can be written in the form (cf. Truesdell and Noll (1965))

$$\begin{aligned} L_{\mathbf{v}} \alpha = & \eta_1 \mathbf{d}^p + \eta_2 \tilde{\tau} + \eta_3 \mathbf{d}^{p^2} + \eta_4 \tilde{\tau}^2 + \eta_5 (\mathbf{d}^p \cdot \tilde{\tau} + \tilde{\tau} \cdot \mathbf{d}^p) \\ & + \eta_6 (\mathbf{d}^{p^2} \cdot \tilde{\tau} + \tilde{\tau} \cdot \mathbf{d}^{p^2}) + \eta_7 (\mathbf{d}^p \cdot \tilde{\tau}^2 + \tilde{\tau}^2 \cdot \mathbf{d}^p) \\ & + \eta_8 (\mathbf{d}^{p^2} \cdot \tilde{\tau}^2 + \tilde{\tau}^2 \cdot \mathbf{d}^{p^2}), \end{aligned} \quad (4.28)$$

where η_1, \dots, η_8 are functions of the basic invariant of \mathbf{d}^p and $\tilde{\tau}$, the porosity parameter ξ and temperature ϑ .

A linear approximation of the general evolution law (4.28) leads to the result

$$\mathbf{L}_\nu \boldsymbol{\alpha} = \eta_1 \mathbf{d}^p + \eta_2 \tilde{\tau}. \quad (4.29)$$

This kinetic law represents the linear combination of the Prager and Ziegler kinematic hardening rules.

To determine the connection between the material functions η_1 and η_2 we take advantage of the geometrical relation (cf. Duszek and Perzyna (1991a))

$$(\mathbf{L}_\nu \boldsymbol{\alpha} - r \mathbf{d}^p) : \mathbf{Q} = 0, \quad (4.30)$$

where

$$\mathbf{Q} = \left[\frac{\partial f}{\partial \boldsymbol{\tau}} + \left(\frac{\partial f}{\partial \xi} - \frac{\partial \kappa}{\partial \xi} \right) \frac{\partial \xi}{\partial \boldsymbol{\tau}} \right] \left\| \left[\frac{\partial f}{\partial \boldsymbol{\tau}} + \left(\frac{\partial f}{\partial \xi} - \frac{\partial \kappa}{\partial \xi} \right) \frac{\partial \xi}{\partial \boldsymbol{\tau}} \right] \right\|^{-1}, \quad (4.31)$$

and r denotes the new material function.

The relation (4.30) leads to the result

$$\eta_2 = \frac{1}{T_m} \langle \Phi(\frac{f}{\kappa} - 1) \rangle [r(\xi, \vartheta) - \eta_1] \frac{\mathbf{P} : \mathbf{Q}}{\tilde{\tau} : \mathbf{Q}}. \quad (4.32)$$

Finally the kinematic hardening evolution law takes the form

$$\mathbf{L}_\nu \boldsymbol{\alpha} = \frac{1}{T_m} \langle \Phi(\frac{f}{\kappa} - 1) \rangle \left[r_1(\xi, \vartheta) \mathbf{P} + r_2(\xi, \vartheta) \frac{\mathbf{P} : \mathbf{Q}}{\tilde{\tau} : \mathbf{Q}} \tilde{\tau} \right], \quad (4.33)$$

where

$$r_1(\xi, \vartheta) = \eta_1, \quad r_2(\xi, \vartheta) = r - \eta_1. \quad (4.34)$$

It is noteworthy to add that the developed procedure can be used as general approach for obtaining various particular kinematic hardening laws. As an example let us assume that the evolution function A in (4.27) instead of \mathbf{d}^p and $\tilde{\tau}$ depends on \mathbf{d}^p and $\boldsymbol{\alpha}$ only (cf. Agah–Tehrani et al. (1987)). Then instead of (4.33) we obtain

$$\mathbf{L}_\nu \boldsymbol{\alpha} = \frac{1}{T_m} \langle \Phi(\frac{f}{\kappa} - 1) \rangle [\zeta_1(\xi, \vartheta) \mathbf{P} - \zeta_2(\xi, \vartheta) \boldsymbol{\alpha}], \quad (4.35)$$

where

$$\zeta_1 = r_1, \quad \zeta_2 = -r_2(\xi, \vartheta) \frac{\mathbf{P} : \mathbf{Q}}{\boldsymbol{\alpha} : \mathbf{Q}}. \quad (4.36)$$

When the infinitesimal deformations and rate independent response of a material are assumed and the intrinsic micro–damage effects are neglected then the kinematic hardening law (4.35) reduces to that proposed by Armstrong and Frederick (1966).

The kinematic hardening law (4.35) leads to the nonlinear stress–strain relation with the characteristic saturation effect. The material function $\zeta_1(\xi, \vartheta)$ for $\xi = \xi_0$ and $\vartheta = \vartheta_0$ can be interpreted as an initial value of the kinematic hardening modulus and the material function $\zeta_2(\xi, \vartheta)$ determines the character of the nonlinearity of kinematic hardening. The particular forms of the functions ζ_1 and ζ_2 have to take into account the degradation nature of the influence of the intrinsic micro–damage process on the evolution of anisotropic hardening.

4.6. Thermodynamic restrictions and rate type constitutive relations

Suppose the axiom of the entropy production holds. Then the constitutive assumption (4.1) and the evolution equations (4.13) lead to the results as follows

$$\boldsymbol{\tau} = \rho_{Ref} \frac{\partial \hat{\psi}}{\partial \mathbf{e}}, \quad \eta = -\frac{\partial \hat{\psi}}{\partial \vartheta}, \quad -\frac{\partial \hat{\psi}}{\partial \boldsymbol{\mu}} \cdot \mathbf{L}_v \boldsymbol{\mu} - \frac{1}{\rho \vartheta} \mathbf{q} \cdot \text{grad} \vartheta \geq 0. \quad (4.37)$$

The rate of internal dissipation is determined by

$$\vartheta \hat{i} = -\frac{\partial \hat{\psi}}{\partial \boldsymbol{\mu}} \cdot \mathbf{L}_v \boldsymbol{\mu} = -\left[\frac{\partial \hat{\psi}}{\partial \epsilon^p} \sqrt{\frac{2}{3}} + \frac{\partial \hat{\psi}}{\partial \boldsymbol{\alpha}} : \left(r_1 \mathbf{P} + r_2 \frac{\mathbf{P} : \mathbf{Q}}{\tilde{\boldsymbol{\tau}} : \mathbf{Q}} \tilde{\boldsymbol{\tau}} \right) \right] \Lambda - \frac{\partial \hat{\psi}}{\partial \xi} \Xi. \quad (4.38)$$

Operating on the stress relation (4.37)₁ with the Lie derivative and keeping the internal state vector constant, we obtain (cf. Duszek–Perzyna and Perzyna (1994))

$$\mathbf{L}_v \boldsymbol{\tau} = \mathcal{L}^e : \mathbf{d} - \mathcal{L}^{th} \dot{\vartheta} - [(\mathcal{L}^e + \mathbf{g}\boldsymbol{\tau} + \boldsymbol{\tau}\mathbf{g} + \mathcal{W}) : \mathbf{P}] \frac{1}{T_m} \langle \Phi(\frac{f}{\kappa} - 1) \rangle, \quad (4.39)$$

where

$$\mathcal{L}^e = \rho_{Ref} \frac{\partial^2 \hat{\psi}}{\partial \mathbf{e}^2}, \quad \mathcal{L}^{th} = -\rho_{Ref} \frac{\partial^2 \hat{\psi}}{\partial \mathbf{e} \partial \vartheta}, \quad \mathcal{W} = \eta^* [(\mathbf{g}\boldsymbol{\tau} - \boldsymbol{\tau}\mathbf{g}) : (\boldsymbol{\alpha}\mathbf{g} - \mathbf{g}\boldsymbol{\alpha})]. \quad (4.40)$$

Substituting $\dot{\psi}$ into the energy balance equation and taking into account the results (4.37)₃ and (4.38) gives

$$\rho \vartheta \dot{\eta} = -\text{div} \mathbf{q} + \rho \vartheta \hat{i}. \quad (4.41)$$

Operating on the entropy relation (4.37)₂ with the Lie derivative and substituting the result into (4.41) we obtain

$$\rho c_p \dot{\vartheta} = -\text{div} \mathbf{q} + \vartheta \frac{\rho}{\rho_{Ref}} \frac{\partial \boldsymbol{\tau}}{\partial \vartheta} : \mathbf{d} + \rho \chi^* \boldsymbol{\tau} : \mathbf{d}^p + \rho \chi^{**} \dot{\xi}, \quad (4.42)$$

where the specific heat

$$c_p = -\vartheta \frac{\partial^2 \hat{\psi}}{\partial \vartheta^2} \quad (4.43)$$

and the irreversibility coefficients χ^* and χ^{**} are determined by

$$\begin{aligned}\chi^* &= - \left[\left(\frac{\partial \hat{\psi}}{\partial \in^p} - \vartheta \frac{\partial^2 \hat{\psi}}{\partial \vartheta \partial \in^p} \right) \sqrt{\frac{2}{3}} + \right. \\ &\quad \left. + \left(\frac{\partial \hat{\psi}}{\partial \alpha} - \vartheta \frac{\partial^2 \hat{\psi}}{\partial \vartheta \partial \alpha} \right) : \left(r_1 \mathbf{P} + r_2 \frac{\mathbf{P} : \mathbf{Q}}{\tilde{\tau} : \mathbf{Q}} \tilde{\tau} \right) \right] \frac{1}{\tau : \mathbf{P}}, \\ \chi^{**} &= - \left(\frac{\partial \hat{\psi}}{\partial \xi} - \vartheta \frac{\partial^2 \hat{\psi}}{\partial \vartheta \partial \xi} \right).\end{aligned}\tag{4.44}$$

4.7. Fracture criterion based on the evolution of microdamage

We base the fracture criterion on the evolution of the porosity internal state variable ξ . The volume fraction porosity ξ takes account for microdamage effects.

Let us assume that for $\xi = \xi^F$ catastrophe takes place (cf. Perzyna (1984)), that is

$$\kappa = \hat{\kappa}(\in^p, \vartheta, \xi)|_{\xi=\xi^F} = 0.\tag{4.45}$$

It means that for $\xi = \xi^F$ the material loses its carrying capacity. The condition (4.45) describes the main feature observed experimentally that the load tends to zero at the fracture point.

It is noteworthy that the isotropic hardening–softening material function $\hat{\kappa}$ proposed in Eq. (4.15)₁ should satisfy the fracture criterion (4.45).

5. NUMERICAL SOLUTION OF THE INITIAL – BOUNDARY VALUE PROBLEM (EVOLUTION PROBLEM)

5.1. Adiabatic inelastic flow process

5.1.1. Formulation of an adiabatic inelastic flow process

Let us define an adiabatic inelastic flow process as follows (cf. Perzyna (1994, 1995) and Łodygowski and Perzyna (1997a,b)). Find ϕ , \mathbf{v} , ρ , $\boldsymbol{\tau}$, α , ξ and ϑ as function of t and \mathbf{x} such that

(i) the field equations

$$\begin{aligned}\dot{\phi} &= \mathbf{v}, \\ \dot{\mathbf{v}} &= \frac{1}{\rho_{Ref}} \left(\frac{\boldsymbol{\tau}}{\rho} \text{grad} \rho + \text{div} \boldsymbol{\tau} \right), \\ \dot{\rho} &= -\rho \text{div} \mathbf{v}, \\ \dot{\boldsymbol{\tau}} &= \left(\mathcal{L}^e - \frac{\vartheta}{c_p \rho_{Ref}} \mathcal{L}^{th} \frac{\partial \boldsymbol{\tau}}{\partial \vartheta} \right) : \text{sym} \frac{\partial \mathbf{v}}{\partial \mathbf{x}} + 2 \text{sym} \left(\boldsymbol{\tau} : \frac{\partial \mathbf{v}}{\partial \mathbf{x}} \right) \\ &\quad - \frac{1}{T_m} \langle \Phi \left(\frac{f}{\kappa} - 1 \right) \rangle\end{aligned}\tag{5.1}$$

$$\begin{aligned}
& - \left[\left(\mathcal{L}^e + \frac{\chi^*}{\rho c_p} \mathcal{L}^{th} \boldsymbol{\tau} + \mathbf{g} \boldsymbol{\tau} + \boldsymbol{\tau} \mathbf{g} + \mathcal{W} \right) : \mathbf{P} \right] \\
& - \frac{\chi^{**} \Xi}{\rho c_p} \mathcal{L}^{th}, \\
\dot{\boldsymbol{\alpha}} &= 2 \text{sym} \left(\boldsymbol{\alpha} : \frac{\partial \mathbf{v}}{\partial \mathbf{x}} \right) + \frac{1}{T_m} \langle \Phi \left(\frac{f}{\kappa} - 1 \right) \rangle \left[r_1(\xi, \vartheta) \mathbf{P} + r_2(\xi, \vartheta) \frac{\mathbf{P} : \mathbf{Q}}{\tilde{\boldsymbol{\tau}} : \mathbf{Q}} \tilde{\boldsymbol{\tau}} \right], \\
\dot{\xi} &= \Xi, \\
\dot{\vartheta} &= \frac{\vartheta}{c_p \rho_{Ref}} \frac{\partial \boldsymbol{\tau}}{\partial \vartheta} : \text{sym} \frac{\partial \mathbf{v}}{\partial \mathbf{x}} + \frac{1}{T_m} \langle \Phi \left(\frac{f}{\kappa} - 1 \right) \rangle \frac{\chi^*}{c_p} \boldsymbol{\tau} : \mathbf{P} + \frac{\chi^{**}}{c_p} \Xi;
\end{aligned}$$

(ii) the boundary conditions

- (a) displacement ϕ is prescribed on a part ∂_ϕ of $\partial\phi(\mathcal{B})$ and tractions $(\boldsymbol{\tau} \cdot \mathbf{n})^a$ are prescribed on part ∂_τ of $\partial\phi(\mathcal{B})$, where $\partial_\phi \cap \partial_\tau = 0$ and $\overline{\partial_\phi \cup \partial_\tau} = \partial\phi(\mathcal{B})$;
- (b) heat flux $\mathbf{q} \cdot \mathbf{n} = 0$ is prescribed on $\partial\phi(\mathcal{B})$;

(iii) the initial conditions

$\phi, \mathbf{v}, \rho, \boldsymbol{\tau}, \boldsymbol{\alpha}, \xi$ and ϑ are given at each particle $X \in \mathcal{B}$ at $t = 0$;

are satisfied.

This evolution problem can be prescribed in the matrix notation as follows

$$\left. \begin{aligned}
\text{(i)} \quad & \dot{\boldsymbol{\varphi}} = \mathcal{A}(t, \boldsymbol{\varphi}) \boldsymbol{\varphi} + \mathbf{f}(t, \boldsymbol{\varphi}) \\
\text{(ii)} \quad & \boldsymbol{\varphi}(0) = \boldsymbol{\varphi}^0(\mathbf{x}) \text{ — initial conditions} \\
\text{(iii)} \quad & \text{The boundary conditions}
\end{aligned} \right\} \quad (5.2)$$

5.1.2. Basic features of rate dependent plastic model

Rate dependency (viscosity) allows the spatial difference operator in the governing equations to retain its ellipticity and the initial value problem (the Cauchy problem) is well-posed. Viscosity introduces implicitly a length-scale parameter into the dynamical initial-boundary value problem. The theory of viscoplasticity gives the possibility to obtain mesh-insensitive results.

Since the rate independent plastic response is obtained as the limit case when the relaxation time is equal to zero hence the theory of viscoplasticity offers the regularization procedure for the solution of dynamical initial-boundary value problems under cyclic loadings. Due to that we can investigate numerically the fatigue damage.

5.2. Application of finite difference method

Let us consider the evolution problem in the form of (5.2). Let us introduce in the Euclidean space E^3 a regular difference net of nodes (i, j, k) with convective

coordinates $\chi_i^1 = i\Delta\chi^1$, $\chi_j^2 = j\Delta\chi^2$ and $\chi_k^3 = k\Delta\chi^3$, $i, j, k \in N$, where N is a set of natural numbers, cf. Dornowski (1999). Of course, some of the nodes belong to the edge of the body and are used to approximate the boundary conditions. Time is approximated by a discrete sequence of moments $t_n = n\Delta t$, where Δt is time step, $n \in N$.

For all functions $\varphi = \hat{\varphi}(\mathbf{x}, t)$ of the analysed problem (5.2) we postulate the following approximation in the domain $\Delta E = \Delta\chi^1 \times \Delta\chi^2 \times \Delta\chi^3$ of a convective difference mesh (cf. Fig. 6):

$$\begin{aligned} \varphi(\mathbf{x}, t) \cong \varphi_h(\mathbf{x}, t) = & \mathbf{a}_1(t) + \mathbf{a}_2(t)\chi^1 + \mathbf{a}_3(t)\chi^2 + \mathbf{a}_4(t)\chi^3 \\ & \mathbf{a}_5(t)\chi^1\chi^2 + \mathbf{a}_6(t)\chi^1\chi^3 + \mathbf{a}_7(t)\chi^2\chi^3 + \\ & \mathbf{a}_8(t)\chi^1\chi^2\chi^3, \end{aligned} \quad (5.3)$$

$\mathbf{x} \in \Delta\mathcal{S}$.

The functions $\mathbf{a}_1(t), \dots, \mathbf{a}_8(t)$ depend only on time, are determined by the value of the function $\varphi_w(t) = [\varphi_1(t), \dots, \varphi_8(t)]^T$ in the node points of difference mesh, (cf. Fig. 6). Hence the approximation functions (5.3) can be written in the form

$$\varphi_h(\mathbf{x}, t) = \mathbf{N}(\mathbf{x})\varphi_w(t), \quad \mathbf{x} \in \Delta\mathcal{S}, \quad (5.4)$$

where

$$\begin{aligned} N_1(\mathbf{x}) &= q \left(-\Delta\chi^1 + 2\chi^1 \right) \left(-\Delta\chi^2 + 2\chi^2 \right) \left(\Delta\chi^3 - 2\chi^3 \right), \\ N_2(\mathbf{x}) &= q \left(\Delta\chi^1 + 2\chi^1 \right) \left(-\Delta\chi^2 + 2\chi^2 \right) \left(-\Delta\chi^3 + 2\chi^3 \right), \\ N_3(\mathbf{x}) &= q \left(-\Delta\chi^1 + 2\chi^1 \right) \left(\Delta\chi^2 + 2\chi^2 \right) \left(-\Delta\chi^3 + 2\chi^3 \right), \\ N_4(\mathbf{x}) &= q \left(\Delta\chi^1 + 2\chi^1 \right) \left(\Delta\chi^2 + 2\chi^2 \right) \left(\Delta\chi^3 - 2\chi^3 \right), \\ N_5(\mathbf{x}) &= q \left(-\Delta\chi^1 + 2\chi^1 \right) \left(-\Delta\chi^2 + 2\chi^2 \right) \left(\Delta\chi^3 + 2\chi^3 \right), \\ N_6(\mathbf{x}) &= q \left(\Delta\chi^1 + 2\chi^1 \right) \left(\Delta\chi^2 - 2\chi^2 \right) \left(\Delta\chi^3 + 2\chi^3 \right), \\ N_7(\mathbf{x}) &= q \left(\Delta\chi^1 - 2\chi^1 \right) \left(\Delta\chi^2 + 2\chi^2 \right) \left(\Delta\chi^3 + 2\chi^3 \right), \\ N_8(\mathbf{x}) &= q \left(\Delta\chi^1 + 2\chi^1 \right) \left(\Delta\chi^2 + 2\chi^2 \right) \left(\Delta\chi^3 + 2\chi^3 \right), \\ q &= \frac{1}{8\Delta\chi^1\Delta\chi^2\Delta\chi^3}. \end{aligned} \quad (5.5)$$

Equations (5.4) allow to determine values of the function $\varphi_h(\mathbf{x}, t)$ in any point of the difference mesh, $\mathbf{x} \in \Delta\mathcal{S}$. For the central point $\mathbf{x} = \mathbf{x}_0$, $N_1 = \dots = N_8 = \frac{1}{8}$ and $\varphi_h(t) = [\varphi_1(t) + \dots + \varphi_8(t)]\frac{1}{8}$.

By using (5.4) we can determine the matrix of the difference operators which approximate the first partial derivatives of the function $\varphi(\mathbf{x}, t)$ for $\mathbf{x} \in \Delta\mathcal{S}$,

$$\frac{\partial}{\partial \mathbf{x}} \varphi(\mathbf{x}, t) \cong \frac{\partial}{\partial \mathbf{x}} \varphi_h(\mathbf{x}, t) = \frac{\partial}{\partial \mathbf{x}} \mathbf{N}(\mathbf{x})\varphi_w(t) = \mathbf{R}(\mathbf{x})\varphi_w(t). \quad (5.6)$$

The matrix of the difference operator $\mathbf{R}(\mathbf{x})$ for the central point takes the form

$$\begin{aligned} \mathbf{R}(\mathbf{x} = \mathbf{x}_0) &= \left. \frac{\partial}{\partial \mathbf{x}} \mathbf{N}(\mathbf{x}) \right|_{\mathbf{x}=\mathbf{x}_0} = & (5.7) \\ &= \begin{bmatrix} \frac{-1}{\Delta x^1} & \frac{1}{\Delta x^1} & \frac{-1}{\Delta x^1} & \frac{1}{\Delta x^1} & \frac{-1}{\Delta x^1} & \frac{1}{\Delta x^1} & \frac{-1}{\Delta x^1} & \frac{1}{\Delta x^1} \\ \frac{-1}{\Delta x^2} & \frac{-1}{\Delta x^2} & \frac{1}{\Delta x^2} & \frac{1}{\Delta x^2} & \frac{-1}{\Delta x^2} & \frac{-1}{\Delta x^2} & \frac{1}{\Delta x^2} & \frac{1}{\Delta x^2} \\ \frac{-1}{\Delta x^3} & \frac{-1}{\Delta x^3} & \frac{-1}{\Delta x^3} & \frac{-1}{\Delta x^3} & \frac{1}{\Delta x^3} & \frac{1}{\Delta x^3} & \frac{1}{\Delta x^3} & \frac{1}{\Delta x^3} \end{bmatrix}. \end{aligned}$$

In similar way we can find the difference form of the spatial difference operator $\mathcal{A}(t, \varphi)$ of the considered evolution problem (5.2)

$$\mathcal{A}(t, \varphi) \varphi \cong \mathcal{A}(t, \varphi_h) \mathbf{N}(\mathbf{x}) \varphi_w(t) = \mathcal{A}_h(t, \varphi_h) \varphi_w(t), \quad (5.8)$$

hence

$$\mathcal{A}_h(t, \varphi_h) = \mathcal{A}(t, \varphi_h) \mathbf{N}(\mathbf{x}) \quad \text{for } \mathbf{x} \in \Delta \mathcal{S}. \quad (5.9)$$

For the central node, $\mathbf{x} = \mathbf{x}_0$ the difference operator (5.9) depends only on time.

As a result of the proposed approximation of the evolution problem (5.2) with respect to the spatial variables we obtain a set of differential equations with respect to time and difference equations with respect to spatial variables

$$\frac{d \varphi_h(t)}{dt} = \mathcal{A}_h \varphi_w(t) + \mathbf{f}_h(t). \quad (5.10)$$

For the approximation of (5.10) with respect to time we use the evident scheme of the first order in the form

$$\frac{d \varphi_h(t)}{dt} \cong \frac{\varphi_h^{n+1} - \varphi_h^n}{\Delta t} = \mathcal{A}_h \varphi_w^n + \mathbf{f}_h^n. \quad (5.11)$$

The solution of (5.11) is reduced to the realization of the recurrence relation

$$\varphi_h^{n+1} = \mathbf{C}_h(\Delta t) \varphi_w^n + \Delta t \mathbf{f}_h^n. \quad (5.12)$$

The difference operator

$$\mathbf{C}_h(\Delta t) = \Delta t \mathcal{A}_h + \mathbf{N} \quad (5.13)$$

couple dependent variables and various points of difference mesh.

5.3. Stability criterion

In explicit finite difference scheme for a set of the partial differential equations (5.2)(i) of the hiperbolic type the condition of stability is the criterion of Courant–Friedrichs–Lewy, cf. Courant et al. (1928)

$$\begin{aligned} \Delta t_{n,n+1} &\leq \min \left(\frac{\Delta L_{p,q,r}^n}{|c_{p,q,r}^n|} \right), \quad p = 1, 2, 3, \dots, P; & (5.14) \\ q &= 1, 2, 3, \dots, Q; \quad r = 1, 2, 3, \dots, R, \end{aligned}$$

where $\Delta t_{n,n+1}$ denotes time step, $c_{p,q,r}^n$ denotes the velocity of the propagation of the disturbances in the vicinity of the central node (p, q, r) , $\Delta L_{p,q,r}^n$ is the minimum distance between the mesh nodes which are in the vicinity of the node (cf. Fig. 6).

The Courant–Friedrichs–Lewy condition requires that the numerical domain of dependence of a finite–difference scheme include the domain of dependence of the associated partial differential equations, cf. Durran (1999).

5.4. The Lax–Richtmyer equivalence theorem

We can now state the Lax–Richtmyer equivalence theorem (cf. Richtmyer and Morton (1967), Strang and Fix (1973), Dautray and Lions (1993) and Gustafsson, Kreiss and Olinger (1995)).

Theorem. Suppose that the evolution problem (5.2) is well–posed for $t \in [0, t_0]$ and that it is approximated by the scheme (5.12), which we assume consistent. Then the scheme is convergent if and only if it is stable.

The proof of the Lax–Richtmyer equivalence theorem for the case when the partial differential operator \mathcal{A} in (5.2) is independent of φ can be found in Dautray and Lions (1993).

Remark. Let us consider the evolution problem (5.2) with

$$\mathbf{f}(t, \varphi) \neq 0 \quad (5.15)$$

and $\varphi^0 = 0$, and also the corresponding approximation (5.12). We have

$$\varphi_h^{n+1} = \Delta t \sum_{j=1}^n [\mathbf{C}_h(\Delta t)]^{n-j} \mathbf{f}_h^j. \quad (5.16)$$

If \mathcal{A} is the infinitesimal generator of a semigroup $\{\mathbb{F}(t)\}$ we can write

$$\varphi(t) = \int_0^t \mathbb{F}(t-s) \mathbf{f}(s) ds. \quad (5.17)$$

Under suitable hypotheses on the convergence of \mathbf{f}_h^j to $\mathbf{f}(j\Delta t)$ we can show that expression (5.16) converges to (5.17) if the scheme is stable and consistent.

6. PARTICULAR EXAMPLES

6.1. Dynamic, adiabatic and isothermal, cyclic complex loading processes for a thin plate with small rectangular hole

Let us consider dynamic, adiabatic and isothermal, cyclic loading processes for a thin steel plate with small rectangular hole located in the centre. To the upper edge of the plate the normal and parallel displacements are applied while the lower edge is supported rigidly. Both these displacements change in time cyclically, see Fig. 7 (cf. Dornowski and Perzyna (1999, 2000a,c)).

It has been assumed that both displacements have the same character of change in time.

We consider the cyclic displacement constraints in the form of the three different loading characteristics (adiabatic and isothermal) in time, namely slow–fast, equal–equal and fast–slow, cf. Fig. 7. All three types of constraints are represented by positive cycles, pulsating from zero and having the same amplitudes: $\bar{V}_{max} = 0.6$ mm, $\bar{U}_{max} = 0.2$ mm, and the same period. They have different time for tensile deformation T_t and compress deformation T_c in a cycle as it has been shown in Fig. 7. The tensile and compress constraints are described by the sine functions as follows:

$$\left. \begin{array}{l} V_t \\ U_t \end{array} \right\} = \frac{1}{2} \left[\begin{array}{l} \bar{V}_{max} \\ \bar{U}_{max} \end{array} \sin \pi \left(\frac{t}{T_t} - \frac{1}{2} \right) + \begin{array}{l} \bar{V}_{max} \\ \bar{U}_{max} \end{array} \right], \quad t \in (0, T_t), \quad (6.1)$$

$$\left. \begin{array}{l} V_c \\ U_c \end{array} \right\} = \frac{1}{2} \left[\begin{array}{l} \bar{V}_{max} \\ \bar{U}_{max} \end{array} \sin \pi \left(\frac{t}{T_c} + \frac{1}{2} \right) + \begin{array}{l} \bar{V}_{max} \\ \bar{U}_{max} \end{array} \right], \quad t \in (0, T_c). \quad (6.2)$$

The material of a plate is AISI 4340 steel, which is characterized by material constants listed in Table 2. These parameters have been identified in Dornowski (1999) and Dornowski and Perzyna (2000c). It has been assumed very dense mesh, namely $N \times M = 64 \times 64 = 4096$ nodes.

The influence of the wave shape and temperature on the $\sigma^{YY} - e_{YY}$ relation has been shown in Fig. 8 (all results concern the node near the tip of the rectangular hole, see the black quadrangle in Fig. 7). The maximum stress σ^{YY} per cycle as a function of number of cycles is plotted in Fig. 9. The evolution of microdamage ξ_{grow} for different loading processes is presented in Fig. 10. The distribution of the plastic equivalent deformation in the plate after ten cycles in the isothermal slow–fast loading process has been shown in Fig. 11. The distribution of the microdamage ξ_{grow} is presented in Fig. 12. The distribution of temperature in the plate after ten cycles in the adiabatic slow–fast loading process has been shown in Fig. 13.

Table 2. Material constants for AISI 4340 steel

$\kappa_s^* = 809 \text{ MPa},$	$\kappa_s^{**} = 228 \text{ MPa},$	$\kappa_0^* = 598 \text{ MPa},$	$\kappa_0^{**} = 168 \text{ MPa},$
$\delta^* = 14.00,$	$\delta^{**} = 3.94,$	$\beta^* = 9.00,$	$\beta^{**} = 2.53,$
$\vartheta_0 = 293 \text{ K},$	$\xi_F = 0.20,$	$\rho_{Ref} = 7850 \text{ kg/m}^3$	$\mu = 76.92 \text{ GPa},$
$\lambda = 115.38 \text{ GPa},$	$\theta = 12 \cdot 10^{-6} \text{ K}^{-1},$	$T_m = 2.5 \text{ ms},$	$m = 1,$
$\zeta_1^* = 15.00 \text{ GPa},$	$\zeta_1^{**} = 4.22 \text{ GPa}$	$\zeta_2^* = 69.60$	$\zeta_2^{**} = 19.60$
$c_1 = 0.202,$	$c_2 = 6.7 \cdot 10^{-2},$	$b_1 = 1.00$	$b_2 = 1.30$
$\xi_0 = 6 \cdot 10^{-4},$	$\bar{\chi} = 0.85,$	$\bar{\chi} = 0$	$c_p = 455 \text{ J/kg K}$

6.1.1. Analysis of the influence of various effects

(i) Shape of loading waves

From the results presented in Figs. 8–10 it is clearly shown that the accumulation of microdamage distinctly depends on the wave shape of the assumed loading cycle. The condition can be drawn that cycles with longer time of applied tensile stress lead sooner to the softening of the material, cf. Fig. 10. Different strain rate in a cycle for different kind of adiabatic process influences the character of changes of the consider stress. Difference in amplitude of tensile stress for S–F and F–S loadings are implied by viscosity of a material. For all cases the effect of plastic hardening is characteristic. The saturation of hardening is first observed for S–F loading process (after 5 cycles). These conclusions are in good agreement with the experimental observations presented by Sidey and Coffin (1979).

(ii) Softening effects

There are two reasons for softening effects, namely the microdamage mechanisms and thermomechanical coupling. Both these effects are very well visible in the results presented in Fig. 9. For adiabatic process the softening effect is caused by both reasons and is very high, while for isothermal process the softening is generated only by microdamage mechanisms and is smaller. It is noteworthy to stress that the microdamage process is influenced very much by thermomechanical effects. This is very well visible from the results presented in Fig. 9.

6.2. Dynamic, adiabatic, cyclic loading processes for a thin plate with sharp notch

To investigate more precisely the development of fatigue damage and the propagation of the macrocrack let us consider a dynamic adiabatic cyclic loading process for a thin steel plate with sharp notch, as shown in Fig. 14. To the upper edge of the plate cyclic constraint realized by rigid rotation of the edge of the plate

is applied while the lower edge is supported rigidly (cf. Dornowski and Perzyna (2000d)).

It is considered the cyclic rotation constraint in the form of the loading characteristic (adiabatic) in time, namely slow–fast. This type of constraint is represented by positive cycle, pulsating from zero and having the amplitude $\alpha_{max} = 1.2$ deg and the period $T = 4.0$ ms. It has different time for positive rotation $T_p = 3.6$ ms and negative rotation $T_n = 0.4$ ms. The positive and negative rotations are described by the sine functions. The material of the plate is AISI steel (cf. Table 2).

Utilizing the finite difference method for regularized thermo–elasto–viscoplastic model, the numerical investigation of the three–dimensional dynamic adiabatic deformation in a thin plate with sharp notch is presented.

7. LOCALIZATION AND FRACTURE PHENOMENA

7.1. Discussion of the localization of plastic deformation

The results presented in Fig. 11 have clearly shown the localization phenomena of plastic deformation in small two asymmetric regions located near the tips of the rectangular hole. Of course, the localization is very much diffused, what is typical for an elastic–viscoplastic model of a material.

From the examination of the results presented in Figs. 12 and 13 we can draw the conclusion that also the distributions of microdamage and temperature are very much localized.

7.2. Investigation of localized fatigue fracture phenomena

The distribution of the norm of the Kirchhoff stress tensor $\|\boldsymbol{\tau}\|$ for a thin plate with sharp notch for chosen instants during two deformation cycles has been shown in Fig. 15. The results illustrate the formation of the greatest stress zones in the vicinity of the notch. The characteristic unsymmetrical distribution of these zones is a result of the assumed boundary conditions. In Fig. 16 the evolution of the plastic equivalent deformation in the vicinity of the developed fatigue macrocrack is presented. In the initial part of the cyclic deformation process (several cycles), the plastic zone has a characteristic shape (seed of maple). Such a form of the plastic zone has been observed experimentally. For the advanced cyclic deformation process (i.e. when the number of cycles is increased) the plastic zone is very much restricted to the vicinity of the macrocrack. The macrocrack direction is consistent with the least radius direction of the initial plastic zone. The strong concentration of plastic deformation has been seen on the front of the macrocrack. The evolution of temperature is shown in Fig. 17. Zones of increased temperature correspond to the plastic zones. The maximum value of temperature is $\vartheta_{max} = 879$ K. The effect

of such a strong heating of the material results from its mechanical properties, i.e. the high strength steel, $R_m = 1400$ MPa.

In Fig. 18 the evolution of microdamage is presented. The domain of microdamage is limited to the vicinity of the macrocrack. This effect is a result of the strong concentration of microdamage process on the front of the macrocrack. The complex evolution of the plastic rotation is shown in Fig. 4.23. In the domain lying above the macrocrack the plastic rotation has negative value, i.e. the rotation in the left direction in relation to the assumed coordinate system, while in the domain lying below the macrocrack it has positive value. It is noteworthy that the border between these two domains is consistent with the macrocrack direction. The results for the length of macroscopic fatigue damage crack versus number of cycles for various cyclic loading processes (slow–fast ($T_p = 3.6$ ms, $T_n = 0.4$ ms), equal–equal ($T_p = 2.0$ ms, $T_n = 2.0$ ms) and fast–slow ($T_p = 0.4$ ms, $T_n = 3.6$ ms)) have been plotted in Fig. 20. These results have clearly shown that the length of the macroscopic fatigue damage crack distinctly depends on the wave shape of the assumed loading cycle. It has been proved that the most dangerous situation we have for the slow–fast cyclic loading process. This result is in accord with the experimental observations performed by Sidey and Coffin (1979). This conclusion is approved by the comparison of the speed of macroscopic crack propagation for various loading processes, cf. Fig. 21. From this comparison it is clear that the speed value of macroscopic crack propagation for the slow–fast cyclic loading has dominating character almost for the entire process considered.

8. FINAL COMMENTS

We hope that a new constitutive model proposed is sufficiently simple in its nature that it can be applicable to the numerical solution of initial–boundary value problems under cyclic loadings.

The crucial idea in this theory is the very efficient interpretation of a finite set of the internal state variables as the equivalent plastic deformation, volume fraction porosity and the residual stress (the back stress). To describe suitably the time and temperature dependent effects observed experimentally and the accumulation of the plastic deformation and damage during dynamic cyclic loading process the kinetics of microdamage and the kinematic hardening law have been modified. To show how the modification of the evolution equation for the porosity parameter ξ helps to describe the accumulation of damage during dynamic cyclic loading process the evolution of the microdamage ξ_{grow} in a node near the tip of the hole (black quadrangle) for different forms of the stress intensity invariant for adiabatic process and various wave shape loadings is presented in Fig. 22.

The performed numerical simulations of the dynamic, cyclic loading process have proven the usefulness of the thermo–elasto–viscoplastic theory. The vis-

coplastic regularization procedure assures the stable integration algorithm by using the finite difference method. Convergence, consistency, and stability of the discretised problem are discussed. The Lax–Richtmyer equivalence theorem is formulated and conditions under which this theorem is valid are examined. The accumulation of damage and equivalent plastic deformation on each considered cycle has been obtained. It has been numerically found that accumulation of microdamage distinctly depends on the wave shape of the assumed loading cycle.

In a particular numerical example considered (a dynamic, adiabatic, cyclic loading process for a thin plate with sharp notch) small localized region, distributed asymmetrically near the tip of the notch, which undergoes significant deformation and temperature rise has been determined. Its evolution until occurrence of fatigue fracture in the form of a macrocrack has been simulated. The investigation of the propagation macroscopic fatigue damage crack within the material of the plate has shown that the length of the macrocrack distinctly depends also on the wave shape of the assumed loading cycle. This conclusion is approved by the comparison of the speed of macroscopic crack propagation for various loading processes.

Acknowledgment

The paper has been partly prepared within the research programme sponsored by the Committee of Scientific Research under Grant 7 T07 A006 16.

REFERENCES

1. Abraham, R., Marsden, J.E. and Ratiu, T., 1988, *Manifolds, Tensor Analysis and Applications*. Springer, Berlin.
2. Agah–Tehrani, A., Lee, E.H., Malett, R.L. and Onat, E.T., 1987. "The theory of elastic–plastic deformation at finite strain with induced anisotropy modelled isotropic–kinematic hardening", *J. Mech. Phys. Solids* **35**, pp. 43–60.
3. Armstrong, P.J. and Frederick, C.O., 1966, "A mathematical representation of the multiaxial Baushinger effect", CEGB Report RD/B/N731, Central Electricity Generating Board.
4. Auricchio, F., Taylor, R.L. and Lubliner, J., 1992, "Application of a return map algorithm to plasticity models", In *COMPLAS Computational Plasticity: Fundamentals and Applications*, (eds. D.R.J.Owen and E.Onate), Barcelona, pp. 2229–2248.
5. Auricchio, F. and Taylor, R.L., 1995, "Two material models for cyclic plasticity models: Nonlinear kinematic hardening and generalized plasticity", *Int. J. Plasticity* **11**, pp. 65–98.

6. Coleman, B.D. and Noll, W., 1963, "The thermodynamics of elastic materials with heat conduction and viscosity", *Arch. Rational Mech. Anal.* **13**, pp. 167–178.
7. Carroll, M.M. and Holt, A.C., 1972, "Static and dynamic pore-collapse relations for ductile solids", *J. Appl. Phys.* **43**, pp. 1626–1636.
8. Chaboche, J.L., 1986, "Time – independent constitutive theories for cyclic plasticity", *Int. J. Plasticity* **2**, pp. 149–188.
9. Courant, R., Friedrichs, K.O. and Lewy, H., 1928, "Über die partiellen differenzgleichungen der mathematischen physik", *Math. Ann.* **100**, pp. 32–74.
10. Curran, D.R., Seaman, L. and Shockey, D.A., 1987, "Dynamic failure of solids", *Physics Reports* **147**, pp. 253–388.
11. Dafalias, Y.F., 1983, "Corotational rates for kinematic hardening at large plastic deformations", *J. Appl. Mech.* **50**, pp. 561–565.
12. Dafalias, Y.F., 1984, "The plastic spin concept and simple illustration of its rule in final plastic transformations", *Mech. Mater.* **3**, pp. 223.
13. Dafalias, Y.F., 1985, "The plastic spin", *J. Appl. Mech.* **52**, pp. 865–871
14. Dafalias, Y.F., 1987, "Issues on the constitutive formulation at large elasto-plastic deformations, Part 1: Kinematics", *Acta Mechanica* **69**, pp. 119.
15. Dafalias, Y.F., 1988, "Issues on the constitutive formulation at large elasto-plastic deformations, Part 2: Kinetics", *Acta Mechanica* **73**, pp. 121.
16. Dafalias, Y.F. and Popov, E.P., 1976, "Plastic internal variable formalism of cyclic plasticity", *J. Appl. Mech.* **43**, pp. 645–651.
17. Dautray, R. and Lions, J.-L., 1993, "Mathematical Analysis and Numerical Methods for Science and Technology", Vol. 6. "Evolution Problems II", Springer, Berlin.
18. Dornowski, W., 1999, "Influence of finite deformation on the growth mechanism of microvoids contained in structural metals", *Arch. Mechanics* **51**, pp. 71–86.
19. Dornowski, W., 2000, "An algorithm of numerical integration for thermo-elasto-viscoplastic constitutive equations", *Biul. WAT* **3(571)**, pp. 31–49.
20. Dornowski, W. and Perzyna, P., 1999, "Constitutive modelling of inelastic solids for plastic flow processes under cyclic dynamic loadings", *ASME J. Eng. Materials and Technology* **121**, pp. 210–220.
21. Dornowski, W. and Perzyna, P., 2000a, "Numerical solutions of thermo-viscoplastic flow processes under cyclic dynamic loadings", In: *Proc. Euro-mech Colloquium 383, Inelastic Analysis of Structures under Variable Loads: Theory and Engineering Applications* (Ed. Weichert, D.), Kluwer Academic Publishers, (in print).
22. Dornowski, W. and Perzyna, P., 2000b, "Analysis of the influence of various effects on cycle fatigue damage in dynamic processes", *Arch. Applied Mechanics* (submitted for publication).

23. Dornowski, W. and Perzyna, P., 2000c, "Localization phenomena in thermo-viscoplastic flow processes under cyclic dynamic loadings", *Computer Assisted Mechanics and Engineering Sciences* **7**, pp. 117–160.
24. Dornowski, W. and Perzyna, P., 2000d, "Localized fracture phenomena in thermo-viscoplastic flow processes under cyclic dynamic loadings", *Acta Mechanica* (submitted for publication).
25. Durrant, D.R., 1999, "Numerical Methods for Wave Equations in Geophysical Fluid Dynamics", Springer, New York.
26. Duszek, M.K. and Perzyna, P., 1988a, "Plasticity of damaged solids and shear band localization", *Ing. Arch.* **58**, pp. 330–392.
27. Duszek, M.K. and Perzyna, P., 1988b, "Influence of the kinematic hardening on the plastic flow localization in damaged solids", *Arch. Mech.* **40**, pp. 595–609.
28. Duszek, M.K. and Perzyna, P., 1991a, "On combined isotropic and kinematic hardening effects in plastic flow processes", *Int. J. Plasticity* **7**, pp. 351–363.
29. Duszek, M.K. and Perzyna, P., 1991b, "The localization of plastic deformation in thermoplastic solids", *Int. J. Solids Structures* **27**, pp. 1419–1443.
30. Duszek–Perzyna, M.K. and Perzyna, P., 1994, "Analysis of the influence of different effects on criteria for adiabatic shear band localization in inelastic solids", In *Material Instabilities: Theory and Applications*, ASME Congress, Chicago, 9–11 November 1994 (Eds. R.C.Batra and H.M.Zbib), AMD–Vol. 183/MD–Vol.50, ASME, New York, pp. 59–85.
31. Duszek–Perzyna, M.K. and Perzyna, P., 1998, "Analysis of anisotropy and plastic spin on localization phenomena", *Arch. Appl. Mechanics* **68**, pp. 352–374.
32. Gustafsson, B., Kreiss, H.O. and Olinger, J., 1995, "Time Dependent Problems and Difference Methods", John Wiley, New York.
33. Halphen, B., 1975, "Sur le champ des vitesses en thermoplasticité finie", *Int. J. Solids Structures* **11**, pp. 947.
34. Jaumann, G., 1911, "Geschlossenes System physikalischer und chemischer Differentialgesetze", *Sitzgsber. Akad. Wiss. Wien (IIa)* **120**, pp. 385–530.
35. Johnson, J.N., 1981, "Dynamic fracture and spallation in ductile solids", *J. Appl. Phys.* **52**, pp. 2812–2825.
36. Kratochvil, J., 1971, "Finite-strain theory of crystalline elastic–inelastic materials", *J. Appl. Phys.* **42**, pp. 1104.
37. Loret, B., 1983, "On the effect of plastic rotation in the finite deformation of anisotropic elastoplastic materials", *Mech. Mater.* **2**, pp. 287–304.
38. Loret, B., 1985, "On the effects of plastic rotation on the localization of anisotropic elastoplastic solids", *Plastic Instability*, (eds. Salencon J. et al.), Presses Ponts et Chausees, Paris, pp.89–100.

39. Łodygowski, T. and Perzyna, P., 1997, "Localized fracture of inelastic polycrystalline solids under dynamic loading processes", *Int. J. Damage Mechanics* **6**, pp. 364–407.
40. Łodygowski, T. and Perzyna, P., 1997, "Numerical modelling of localized fracture of inelastic solids in dynamic loading processes", *Int. J. Num. Meth. Engng.* **40**, pp. 4137–4158.
41. Mandel, J., 1971, *Plasticité Classique et Viscoplasticite*. CISM Lecture Notes No. 97, Udine, Springer–Verlag, Wien.
42. Mandel, J., 1973, "Equations constitutives et directeurs dans les milieux plastiques et viscoplastiques", *Int. J. Solids Structures* **9**, pp. 725–740.
43. Mandel, J., 1982, "Définition d'un repère privilégié pour l'étude des transformations anélastiques du polycrystal", *J. Méc. Théo. Appl.* **1**, pp. 7.
44. Marsden, J.E. and Hughes, T.J.R., 1983, *Mathematical Foundations of Elasticity*. Prentice–Hall, Englewood Cliffs, New York.
45. Mróz, Z., 1967, "On the description of anisotropic workhardening", *J. Mech. Phys. Solids* **15**, pp. 163–175.
46. Needleman, A. and Rice, J.R., 1978, "Limits to ductility set by plastic flow localization", In *Mechanics of Sheet Metal Forming*, Ed. Koistinen, D.P. and Wang, N.M., Plenum, New York, pp. 237–267.
47. Nemat–Nasser, S., 1992, "Phenomenological theories of elastoplasticity and strain localization at high strain rates", *Appl. Mech. Rev.* **45**, pp. S19–S45.
48. Oldroyd, J., 1950, "On the formulation of rheological equations of state", *Proc. Roy. Soc. (London)* **A 200**, pp. 523–541.
49. Perzyna, P., 1963, "The constitutive equations for rate sensitive plastic materials", *Quart. Appl. Math.*, **20**, pp. 321–332.
50. Perzyna, P., 1966, "Fundamental problems in viscoplasticity", *Advances in Applied Mechanics* **9**, pp. 343–377.
51. Perzyna, P., 1971, "Thermodynamic theory of viscoplasticity", *Advances in Applied Mechanics* **11**, pp. 313–354.
52. Perzyna, P., 1984, "Constitutive modelling of dissipative solids for postcritical behaviour and fracture", *ASME J. Eng. Materials and Technology* **106**, pp. 410–419.
53. Perzyna, P., 1986a, "Internal state variable description of dynamic fracture of ductile solids", *Int. J. Solids Structures* **22**, pp. 797–818.
54. Perzyna, P., 1986b, "Constitutive modelling for brittle dynamic fracture in dissipative solids", *Arch. Mechanics* **38**, pp. 725–738.
55. Perzyna, P., 1990, "Influence of anisotropic effects on micro–damage process in dissipative solids", In *Yielding, Damage and Failure of Anisotropic Solids*, Proc. IUTAM/ICM Symposium Villerd-de-Lance, August 1987, (ed. J.P.Boehler), Mech. Eng. Publl. Limited, London, pp. 483–507.

56. Perzyna, P., 1994, "Instability phenomena and adiabatic shear band localization in thermoplastic flow processes", *Acta Mechanica*, **106**, pp. 173–205.
57. Perzyna, P., 1995, "Interactions of elastic–viscoplastic waves and localization phenomena in solids", *Nonlinear Waves in Solids, Proc. IUTAM Symposium*, August 15–20, 1993, Victoria, Canada, (eds. L.J. Wegner and F.R. Norwood), ASME Book No AMR 137, pp. 114–121.
58. Perzyna, P. and Drabik, A., 1989, "Description of micro–damage process by porosity parameter for nonlinear viscoplasticity", *Arch. Mechanics* **41**, pp. 895–908.
59. Perzyna, P. and Drabik, A., 2001, "Micro–damage mechanism in adiabatic processes", *Int. J. Plasticity* (submitted for publication).
60. Prager, W., 1955, "The theory of plasticity: A survey of recent achievements", (J. Clayton Lecture), *Proc. Inst. Mech. Eng.* **169**, pp. 41–57.
61. Richtmyer, R.D. and Morton, K.W., 1967, "Difference Methods for Initial–Value Problems", John Wiley, New York.
62. Ristinmaa, M., 1995, "Cyclic plasticity model using one yield surface only", *Int. J. Plasticity* **11**, pp. 163–181.
63. Shima, S. and Oyane, M., 1976, "Plasticity for porous solids", *Int. J. Mech. Sci.* **18**, pp. 285–291.
64. Shockey, D.A., Seaman, L. and Curran, D.R., 1985, "The microstatistical fracture mechanics approach to dynamic fracture problem", *Int. J. Fracture* **27**, pp. 145–157.
65. Sidey, D. and Coffin, L.F., 1979, "Low–cycle fatigue damage mechanisms at high temperature", In *Fatigue Mechanism*, Proc. ASTM STP 675 Symposium, Kansas City, Mo., May 1978, (ed. J.T.Fong), Baltimore, pp. 528–568.
66. Strang, G. and Fix, G.J., 1973, "An Analysis of the Finite Element Method", Prentice–Hall, Englewood Cliffs.
67. Truesdell C. and Noll W., 1965, "The nonlinear field theories", *Handbuch der Physik*, Band III/3, Springer, Berlin, pp. 1–579.
68. Van der Giessen, E., 1989, "Continuum models of large deformation plasticity, Part I: Large deformation plasticity and the concept of a natural reference state", *Eur. J. Mech., A/Solids* **8**, pp. 15.
69. Van der Giessen, E., 1989, "Continuum models of large deformation plasticity, Part II: A kinematic hardening model and the concept of a plastically induced orientational structure", *Eur. J. Mech., A/Solids* **8**, pp. 89.
70. Van der Giessen, E., 1991, "Micromechanical and thermodynamic aspects of the plastic spin", *Int. J. Plasticity* **7**, pp. 365–386.
71. Wang, J.–D. and Ohno, N., 1991, "Two equivalent forms of nonlinear kinematic hardening: application to nonisothermal plasticity", *Int. J. Plasticity* **7**, pp. 637–650.

72. Zaremba, S., 1903, "Sur une forme perfectionnée de la théorie de la relaxation", *Bull. Int. Acad. Sci. Cracovie*, pp. 594–614.
73. Zaremba, S., 1903, "Le principe des mouvements relatifs et les équations de la mécanique physique", *Bull. Int. Acad. Sci. Cracovie*, pp. 614–621.
74. Ziegler, H., 1959, "A modification of Prager's hardening rule", *Quart. Appl. Math.* **17**, pp. 55–65.

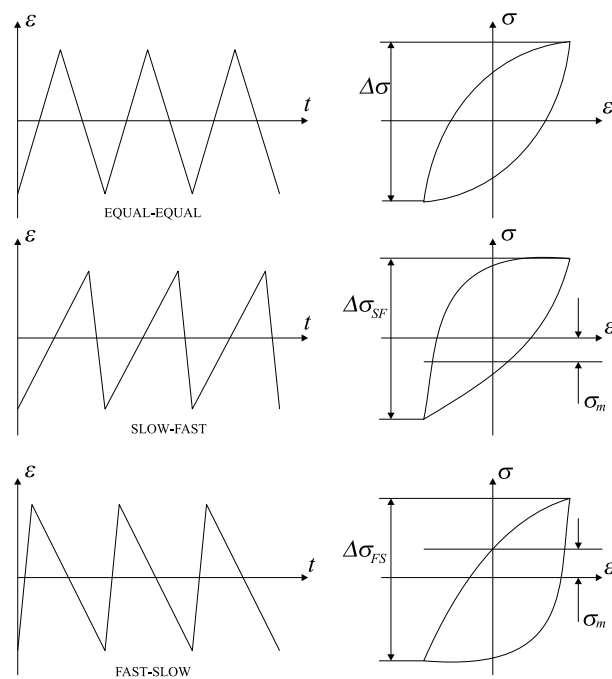


Figure 1. Wave shapes and resulting hysteresis loops for equal and unequal forward and reverse strain rates (After Sidey and Coffin (1979))

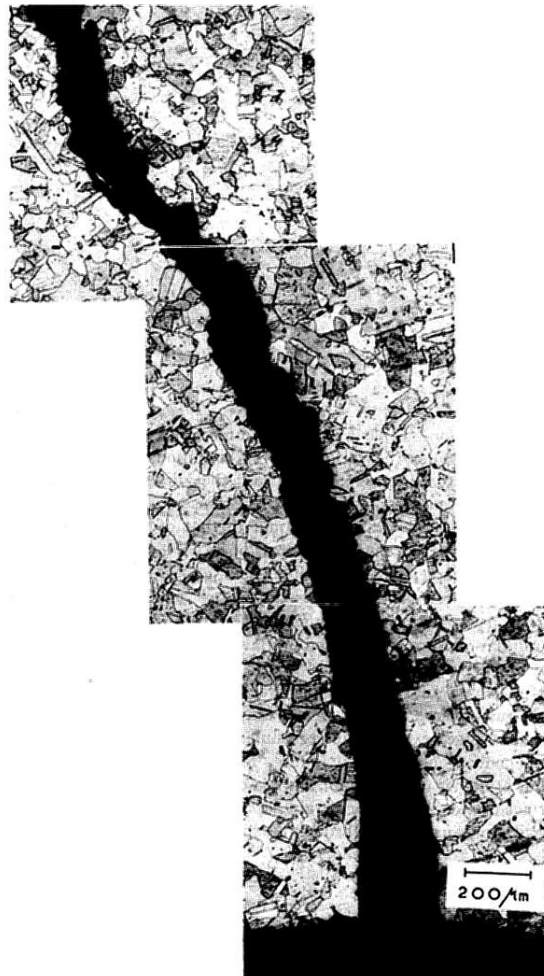


Figure 2. Main failure crack in OFHC copper after fast–slow cycling showing transgranular fracture mode (After Sidey and Coffin (1979))

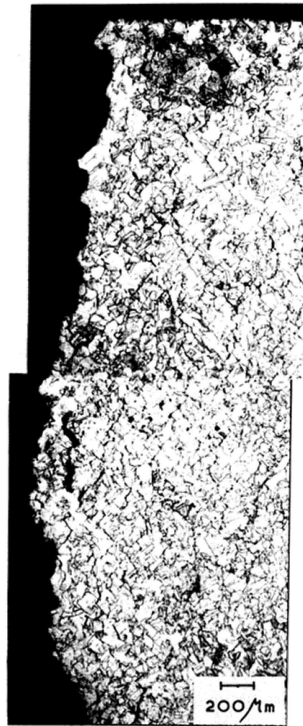


Figure 3. Fracture edge of slow-fast cycle specimen showing intergranular fracture path and surface and interior intergranular cracks (After Sidey and Coffin (1979))

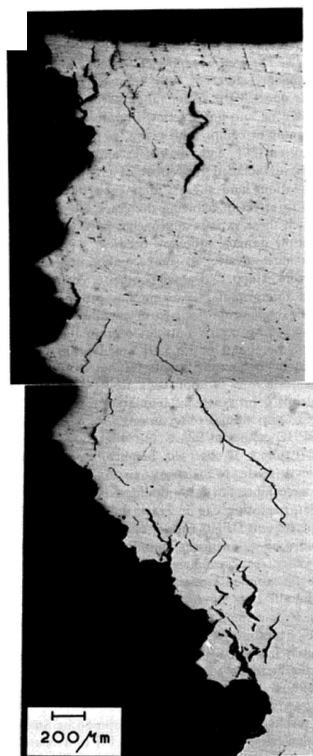


Figure 4. Equal ramp cycle specimen in unetched condition showing interlinkage of wedge cracks near the fracture edge (After Sidey and Coffin (1979))

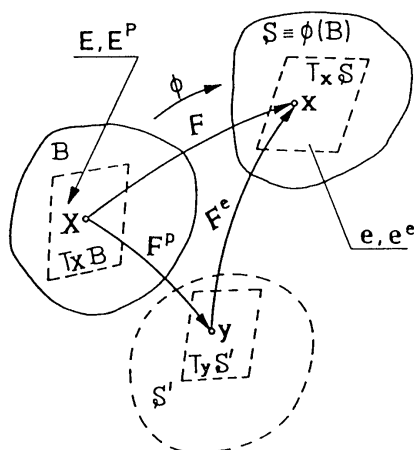


Figure 5. Schematic representation of the multiplicative decomposition by means of the tangent spaces

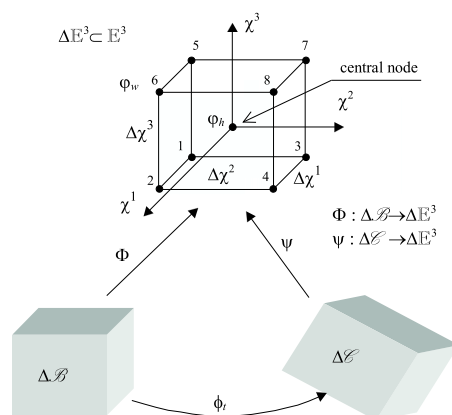


Figure 6. Convective finite difference mesh of nodes

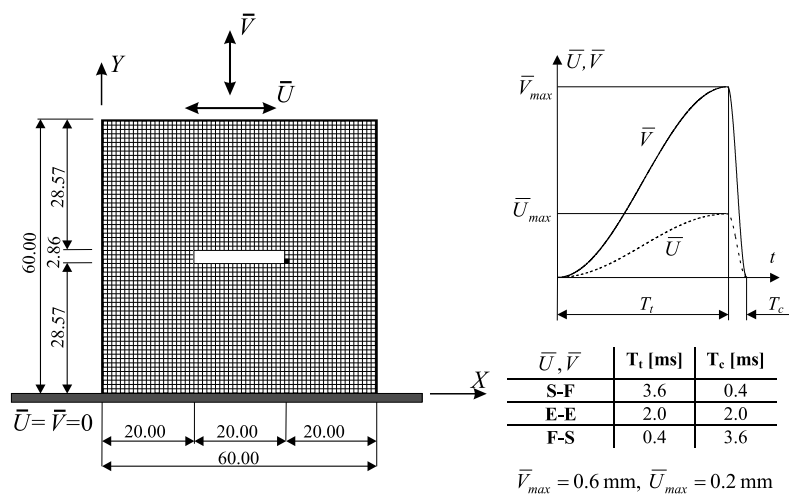


Figure 7. Geometry, kinematic constraints and finite difference discretization (4096 nodes) of the thin steel plate with small rectangular hole located in the center (all dimensions are in millimeters)

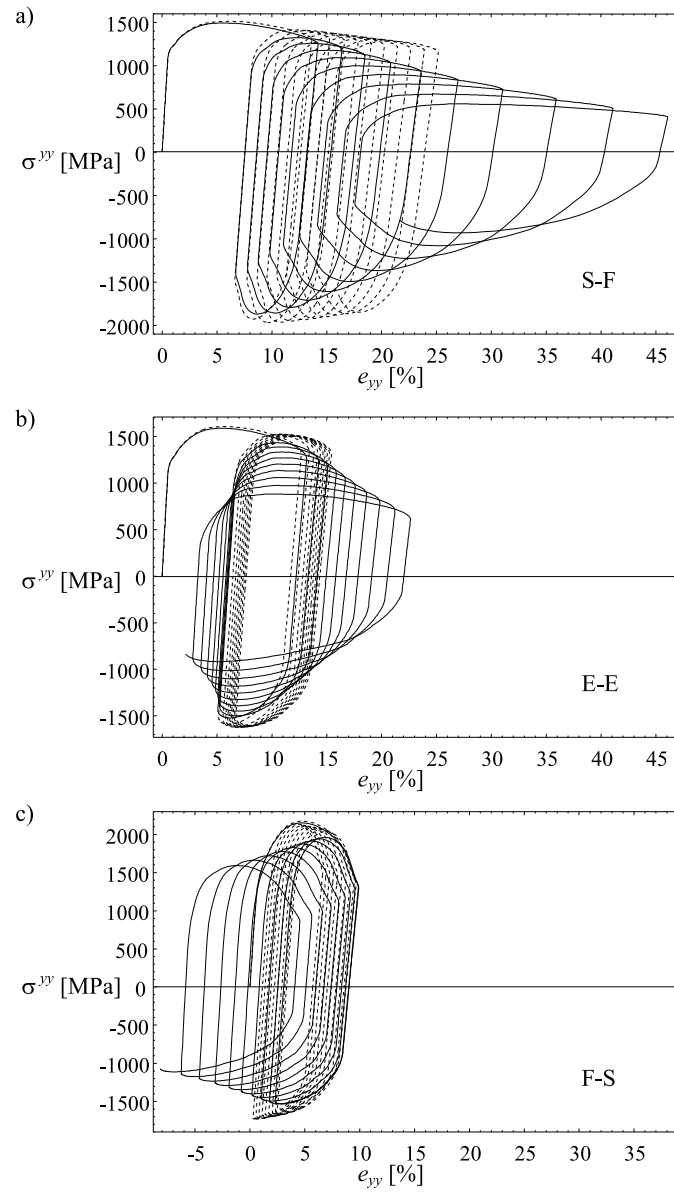


Figure 8. Influence of the wave shape and temperature on the $\sigma^{YY} - e_{YY}$ relation, solid line – adiabatic process, dashed line – isothermal process, (a) slow–fast, (b) equal–equal, (c) fast–slow

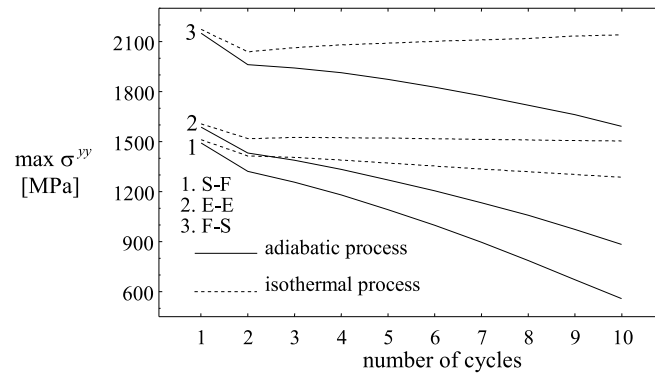


Figure 9. Maximum stress σ^{YY} per cycle as a function of number of cycles

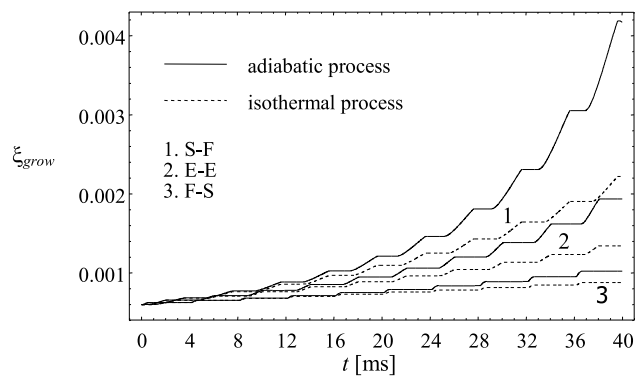


Figure 10. Evolution of the damage ξ_{grow} for different loading processes

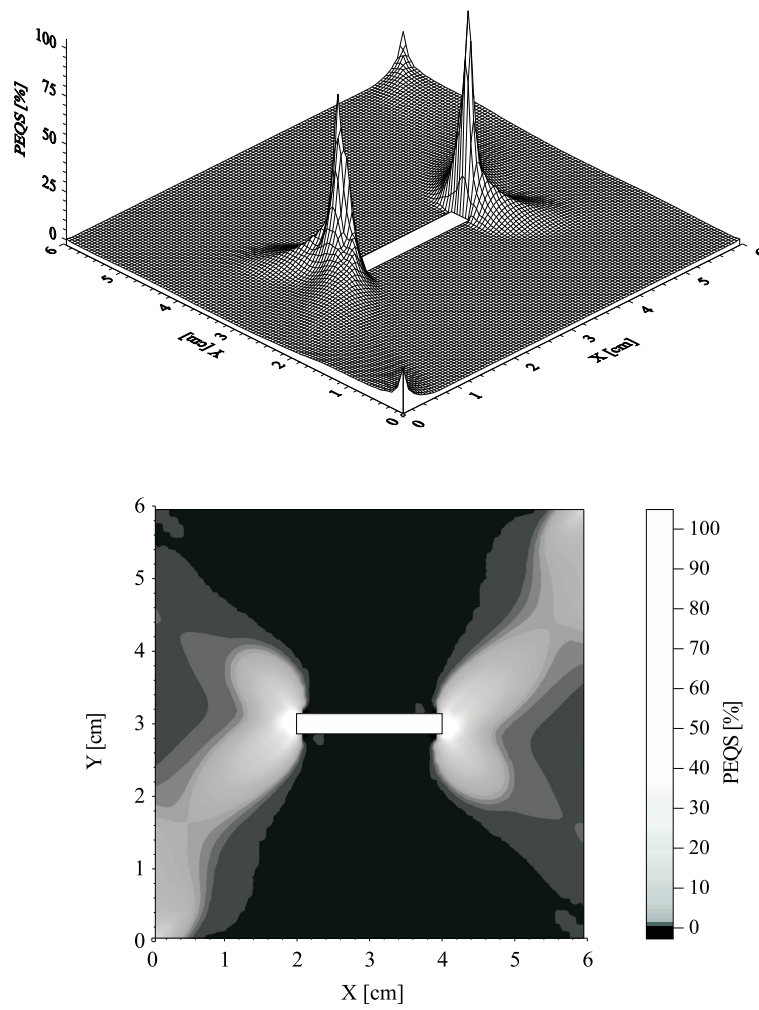


Figure 11. Distribution of the plastic equivalent strain in the plate after ten cycles of the isothermal slow-fast process

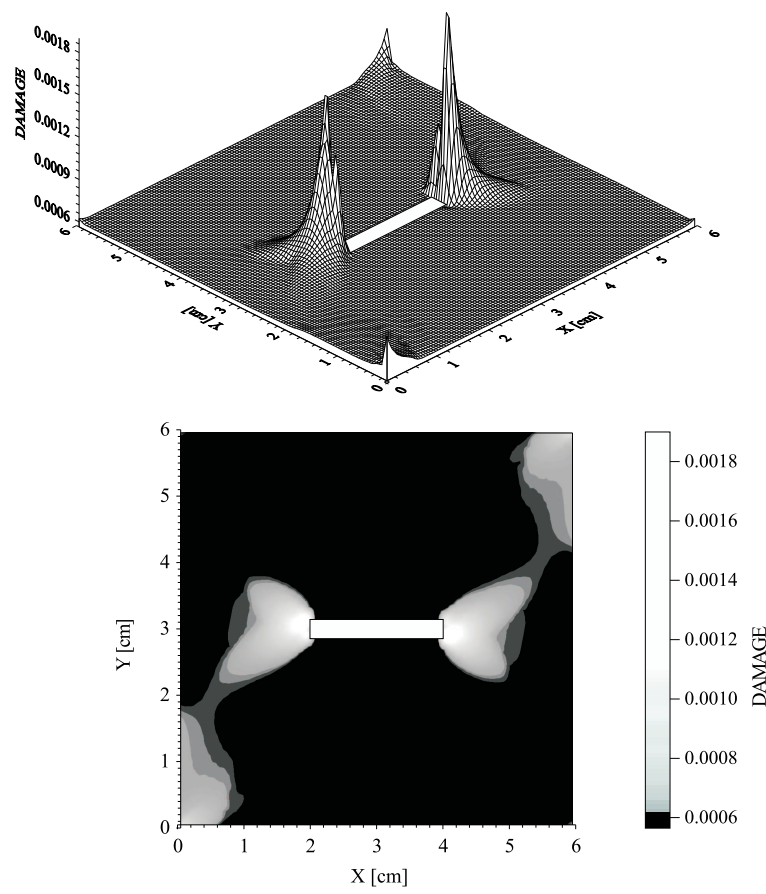


Figure 12. Distribution of the microdamage ξ_{grow} in the plate after ten cycles of the isothermal slow–fast process

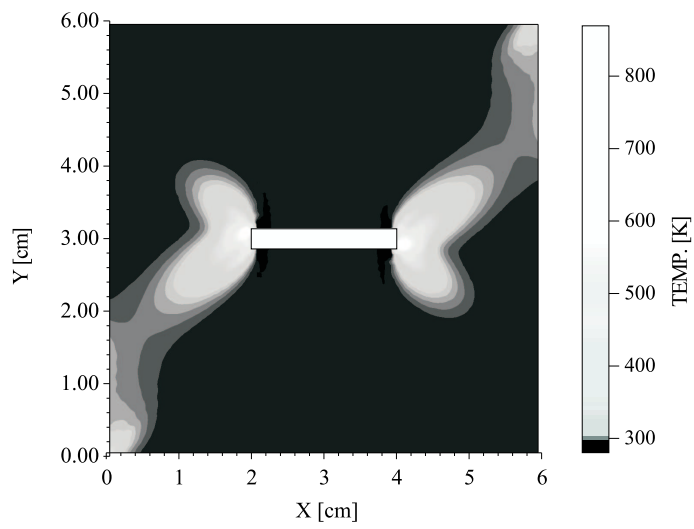
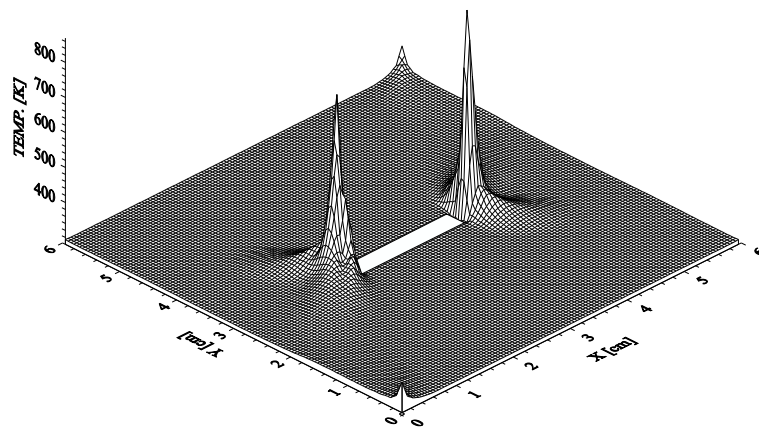


Figure 13. Distribution of temperature ϑ in the plate after ten cycles of the adiabatic slow-fast process

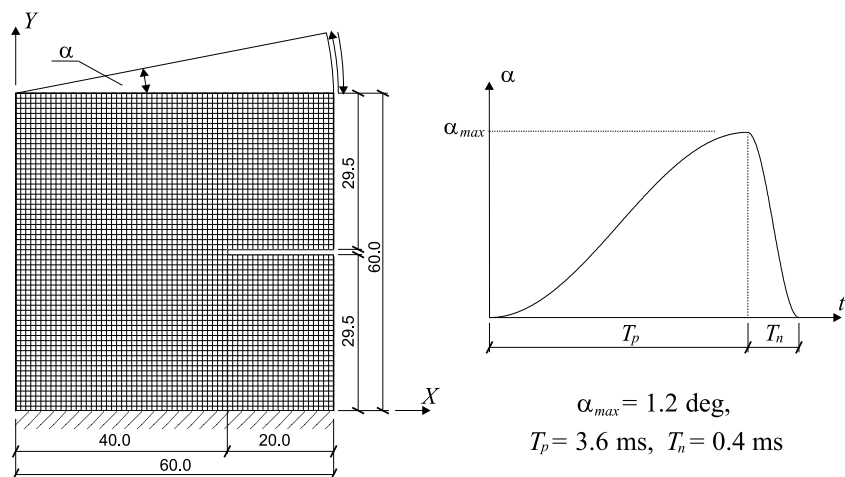


Figure 14. Geometry and kinematic constraints of the thin steel plate with sharp notch

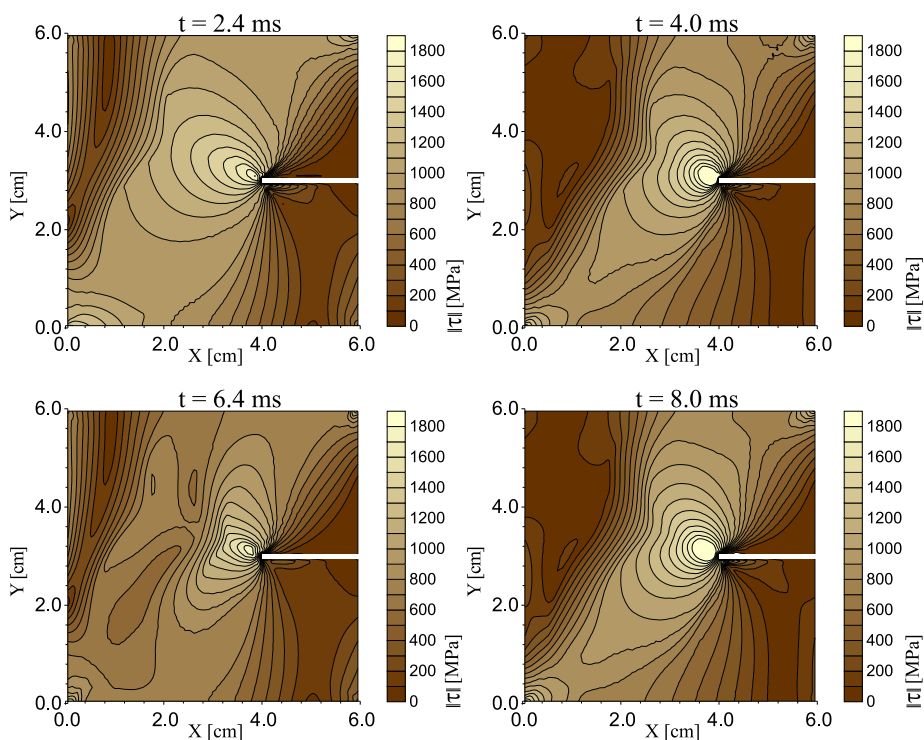


Figure 15. Distribution of the norm of the Kirchhoff stress for chosen instants during two deformation cycles

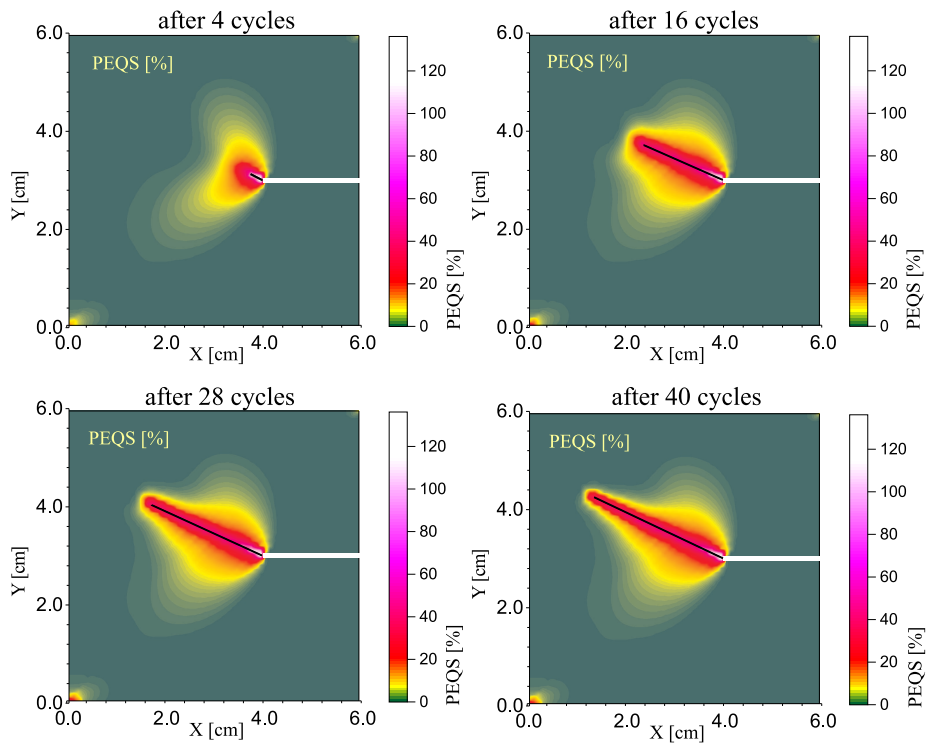


Figure 16. Evolution of the equivalent plastic deformation in the vicinity of the developed fatigue damage

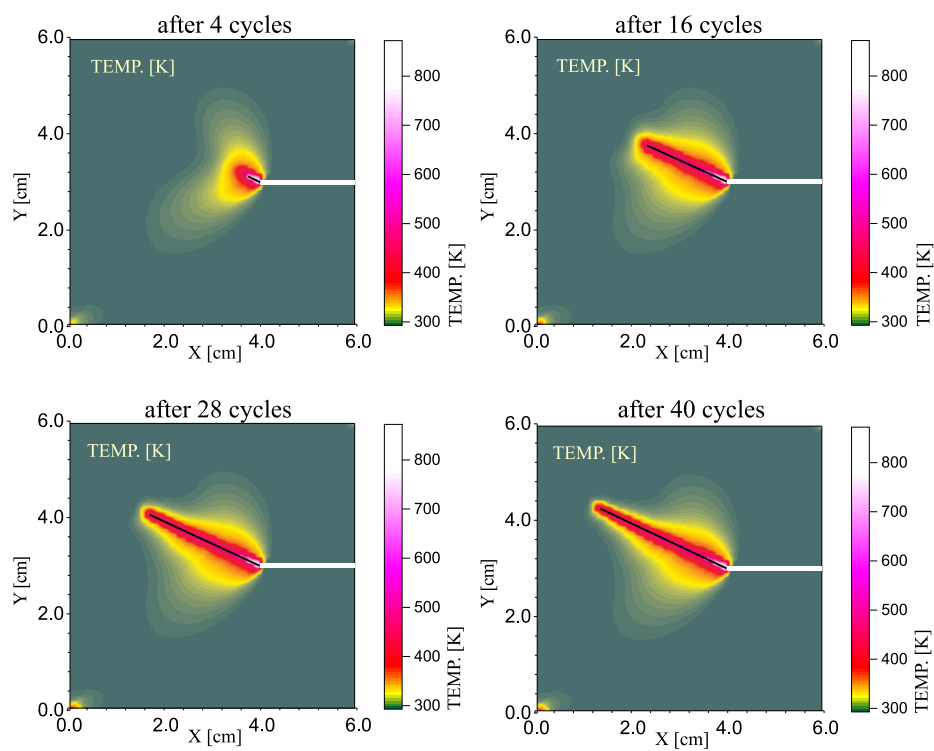


Figure 17. Evolution of temperature in the vicinity of the developed fatigue damage

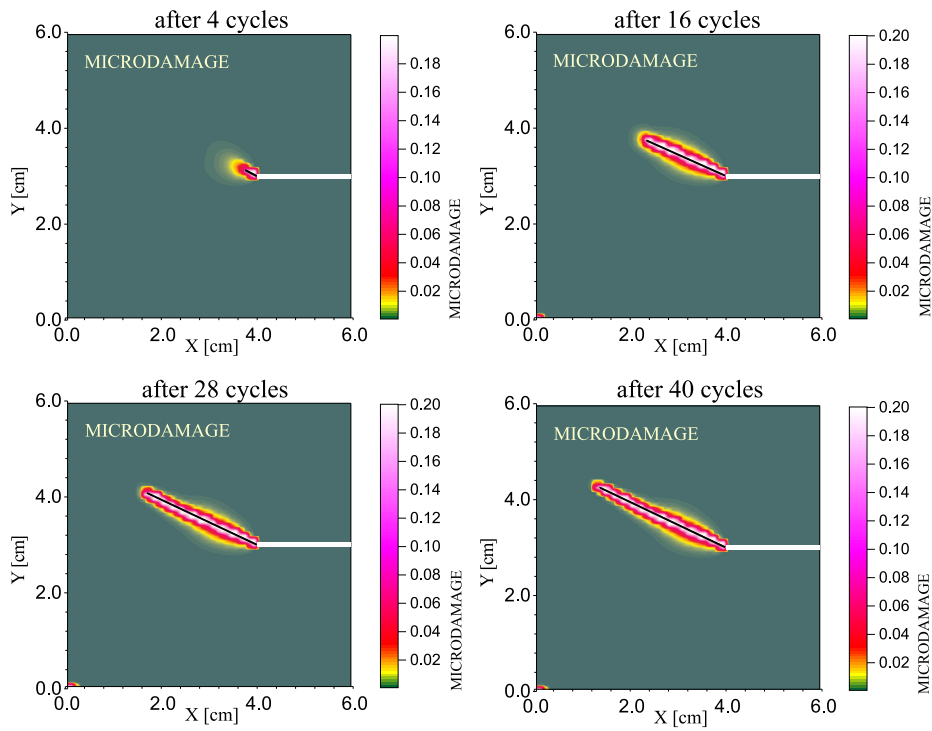


Figure 18. Evolution of the microdamage in the vicinity of the developed fatigue macrocrack

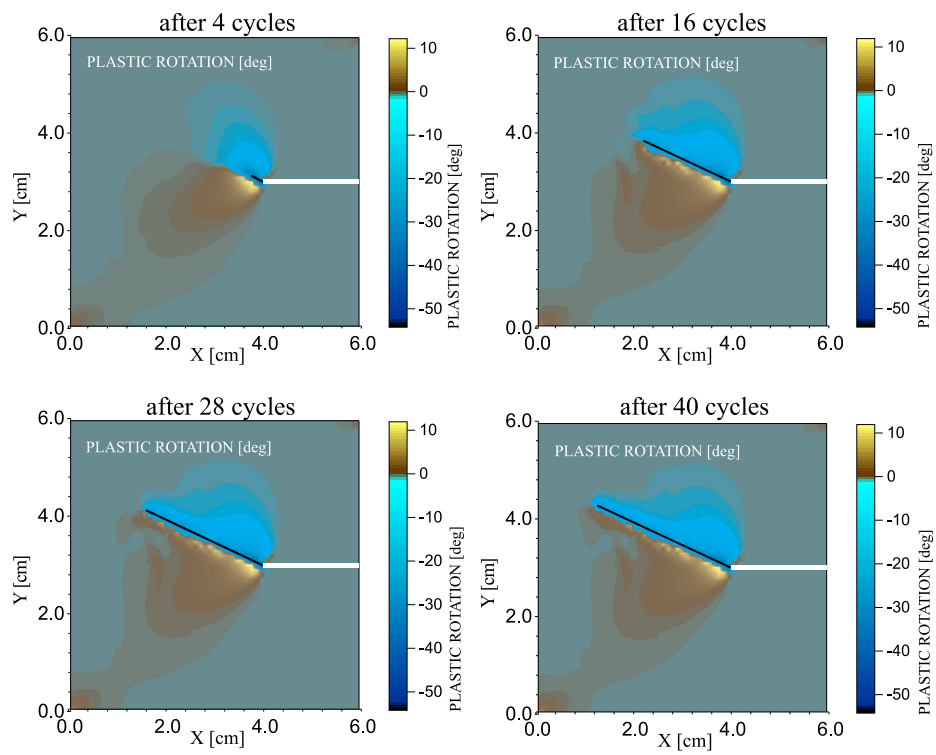


Figure 19. Evolution of the plastic rotation in the vicinity of the developed fatigue macro-crack

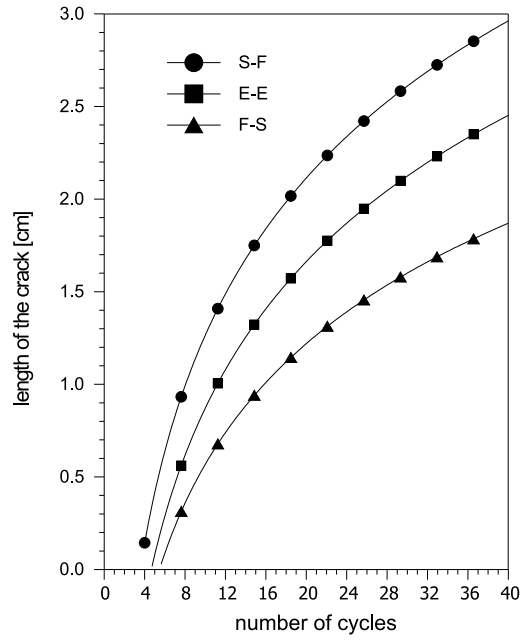


Figure 20. The length of macroscopic fatigue damage crack versus number of cycles for various loading processes

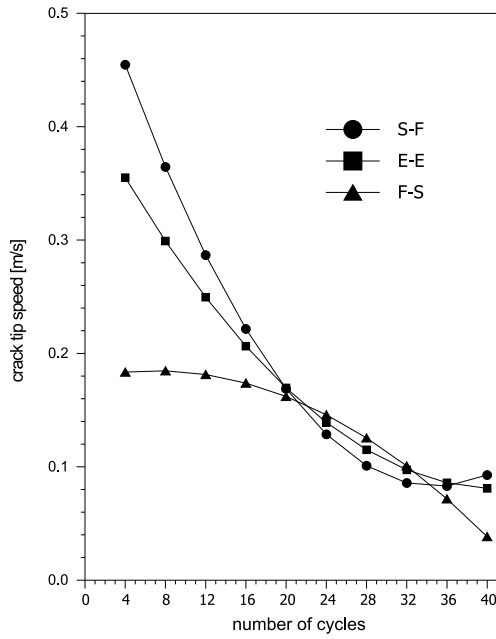


Figure 21. The speed of macroscopic crack propagation versus number of cycles for various loading processes

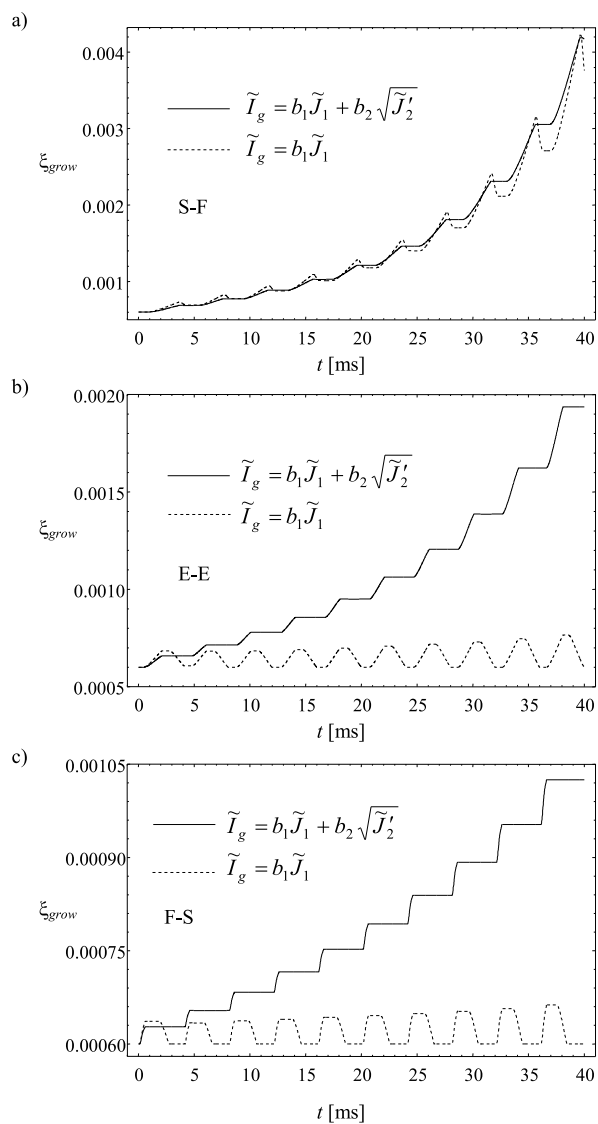


Figure 22. Evolution of the damage ξ_{grow} for different forms of the stress intensity invariant (adiabatic process), (a) slow-fast, (b) equal-equal, (c) fast-slow